RESEARCH ARTICLE

A Compendium of Methodically Determined Ground- and Excited-State Properties of Homoleptic Ruthenium(II) and Osmium(II) Photosensitizers

Felix Glaser,[a] Simon De Kreijger,[a] Katerina Achilleos,[a] Lakshmi Narayan Satheesh,[a] Alexia Ripak,[a] Noémie Chantry,[a] Céline Bourgois,[a] Sophie Quiquempoix,[a] Joffrey Scriven,[a] Julien Rubens,[a] Milan Vander Wee-Léonard,[a] Martin Daenen,[a] Martin Gillard,[a] Benjamin Elias[a] and Ludovic Troian-Gautier[a],[b]*

[a] Dr. F. Glaser, S. De Kreijger, K. Achilleos, L. N. Satheesh, A. Ripak, N. Chantry, C. Bourgois, S. Quiquempoix, J. Scriven, J. Rubens, Dr. M. Vander Wee-Léonard, M. Daenen, Dr. M. Gillard, Prof. Dr. B. Elias, Prof. Dr. L. Troian-Gautier
Institut de la Matière Condensée et des Nanosciences (IMCN), Molecular Chemistry, Materials and Catalysis (MOST)
Université catholique de Louvain (UCLouvain)
Place Louis Pasteur 1 box L4.01.02, B-1348 Louvain-la-Neuve, Belgium
E-mail: Ludovic.Troian@uclouvain.be

[b] Prof. Dr. L. Troian-Gautier
Wel Research Institute
Avenue Pasteur 6, 1300 Wavre, Belgium

Supporting information for this article is given via a link at the end of the document.

Abstract: The one-pot synthesis of a total of 32 ruthenium(II) and osmium(II) photosensitizers bearing substituted 2,2'-bipyridines, 1,10-phenanthrolines, and diaza ligands is reported. Whereas most of these photosensitizers were already reported in the literature, the present study offers extensive datasets of ground- and excited-state properties highly desirable for future development in e.g., machine learning, artificial intelligence, and photoredox catalysis. All photosensitizers absorbed light intensely in the visible part of the spectrum, with the Os(II) photosensitizers absorbing further into the red part. Excited-state lifetimes and photoluminescence quantum yields were generally larger for Ru(II) photosensitizers than for Os(II) analogs, which agrees with the energy gap law. The excited-state redox potentials were determined for all investigated photosensitizers covering a range of –0.21 to –1.35 V *vs* SCE for excited-state oxidation and 0.14 to 1.48 V *vs* SCE for excited-state reduction. A procedure for counter-ion exchange to generate the corresponding PF_6^-, Cl^-, BF_4^-, NO_3^-, OTf^-, ClO_4^-, and BAr^{F-} is reported for six photosensitizers. The synthetic ease, detailed report of fundamental photophysical properties, and a broad range of excited-state redox potentials open opportunities for systematic investigations in several applications and further streamline developments in photoredox catalysis.

Introduction

Photoredox catalysis has become increasingly important in recent years in various fields of chemistry and research applications that take advantage of light as the energy source. Even if the diversity of organic photosensitizers is rapidly expanding,[1–4] transition-metal complexes based on Ru(II), Os(II), and Ir(III) centers still represent the most prominent class of photosensitizers used for such applications, despite their known scarcity.[5] Among these, polypyridine ligands are established as versatile chelating ligand scaffolds that can coordinate many metal centers.[6–10] This results in the formation of photosensitizers with tunable ground and excited-state potentials and excited-state lifetimes that usually range from the nanosecond to the microsecond timescale.[11] This includes famous metal-to-ligand charge transfer (MLCT) excited states with octahedral d^6 and tetragonal d^{10} metal complexes, metal-centered spin-flip states or other metal-centered excited states, especially with first-row transition metal complexes.[8,12–20] Concerning second and third-row metal complexes, osmium (Os(II)) and ruthenium (Ru(II)) based polypyridyl complexes attracted attention already in the 1950s, both for synthetic reasons and for their excited-state behaviors.[21–24] Among these luminescent complexes, the most celebrated example is probably the prototypical $[Ru(bpy)_3]^{2+}$ photosensitizer, where bpy is 2,2'-bipyridine, initially reported by F. H. Burstall in 1936.[25] Their success as photosensitizers in light-induced transformation originated from their relatively easy preparation, the ability to efficiently tune the ground and excited-state properties, and the ability to access homoleptic and heteroleptic complexes with different scaffolds in a comparably small number of steps.[26] This is also reflected by recent reports of ruthenium-based polypyridyl complexes, among others, for light-driven catalysis,[27] multi-photon catalysis,[28,29] solar cells,[18] and anticancer treatment[30,31] like photodynamic therapy.[32,33] Osmium-based derivatives have also been investigated recently, for example for sensitized triplet-triplet annihilation upconversion,[34–36] (metallo)photoredox catalysis,[37,38] multi-photon catalysis,[39,40] energy harvesting and storage[41–43] or photodynamic therapy.[44–48] This versatility in using Ru(II) and Os(II) photosensitizers is also strengthened by findings gained using novel spectroscopic techniques or new reaction concepts and methodologies that have allowed to broaden the scope of light-induced reactivities further.[40,49–52] In addition to their use in academia, transition metal complexes based on Ru(II) and Ir(III) have also received some attention from the life science industry.[53,54]

Here, we describe the synthesis of homoleptic photosensitizers based on Os(II) and Ru(II) metal centers with 16 different ligands (**Figure 1** and **Figure 2**). In most cases, excellent isolated yields were obtained in one step from readily available starting materials following a simple general procedure, with typically limited need for intensive purifications. We also describe the procedure to

isolate these photosensitizers with different counterions, i.e., Cl^-, PF_6^-, ClO_4^-, BF_4^-, BAr^{F-}, NO_3^-, and OTf^-. Most of these photosensitizers are known, and the report of their ground and excited-state behavior spans several decades. However, we believe that, with the growing interest in photoredox catalysis, machine learning, and artificial intelligence, determining ground and excited-state properties under rigorously identical conditions is paramount. As such, the (photo)chemical properties were thoroughly characterized, including the determination of ground and excited-state redox properties, molar absorption coefficients, excited-state lifetimes, photoluminescence quantum yields, and steady-state photoluminescence at 77K. We describe the systematic investigation of ground- and excited-state properties in aerated and deaerated acetonitrile. This compendium of methodically determined ground and excited-state properties of Ru(II) and Os(II) photosensitizers can serve as a reference and be used as a guide for choosing the right photosensitizer for an envisioned application. Note that Ir(III) photosensitizers, which represent one of the most versatile classes of photosensitizers in photoredox catalysis, were not investigated in the present study as the focus was placed on homoleptic $(N^N)_3$ Ru(II) and Os(II) photosensitizers with MLCT excited state. Similar $(N^N)_3$ Ir(III) photosensitizers have been scarcely reported in the literature due to their harsher reaction conditions but often only result in ligand-centered (LC) excited-state transitions.[55–57]

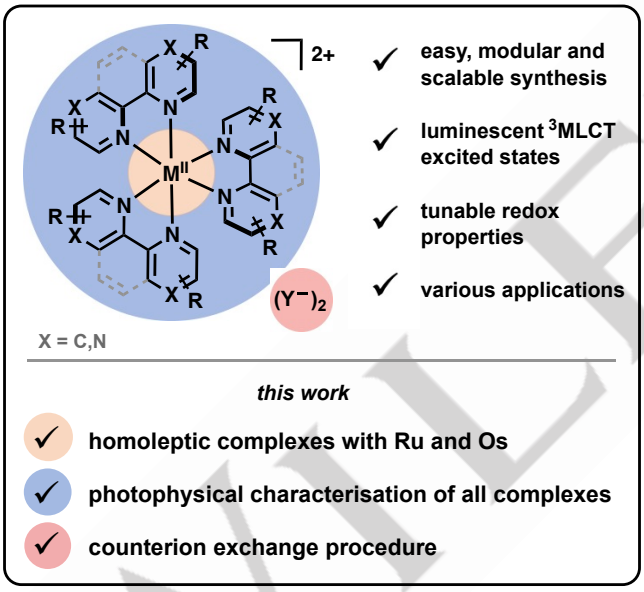

Figure 1. General overview of the research presented herein. The different ligand structures are presented in Figure 2 and the main photophysical properties are summarized in Tables 1 to 3. Y = counterion.

Experimental Section

Materials. Acetonitrile (99.9%, VWR), dichloromethane (99.9%, stabilized with about 0.002% of 2-methyl-2-butene, VWR), diethyl ether (99.9%, VWR), ethanol absolute (99.9%, VWR), acetone (99.9%, VWR), ethylene glycol (≥99.5%, Roth), methanol (99.9%, VWR), n-hexane (97%, VWR), dimethylformamide (99.9%, VWR), butyronitrile (>99.0%, TCI), ammonium hexafluorophosphate (99%, Fluorochem), tetra-n-butylammonium hexafluorophosphate (≥98%, TCI), ammonium chloride (>99%, Acros Organics), aluminium oxide for chromatography (neutral, Brockmann I, 40-300 μm, 60A, Thermo Fisher), silica gel for flash column chromatography (60 Å, 40-63 μm, ROCC), Sephadex-SP C-25 ion exchange resin (40-120 mm, Aldrich), Sephadex LH-20 (Cytiva, 18-111 μm), hydrochloric acid (37%, VWR), sodium chloride (99.5%, Acros Organics), ruthenium(III) chloride hydrate (99%, Ambeed), iron(II) chloride hydrate (99%, Acros Organics), osmium(VIII) tetroxide (99.9%, Pressure Chemicals), 2,2'-bipyridine (98%, Alfa Aesar), 1,10-phenanthroline (99%, Alfa Aesar), 4,7-diphenyl-1,10-phenanthroline (98%, Ambeed), 4,4'-di-*tert*-butyl-2,2'-bipyridine (98%, Ark Pharm), 4,4'-dimethyl-2,2'-bipyridine (98%, Ark Pharm), 5,5'-dimethyl-2,2'-bipyridine (98%, Ark Pharm), 4,4'-dinonyl-2,2'-bipyridine (98%, BLDPharm), 4,4'-dimethoxy-2,2'-bipyridine (99.9%, BLDPharm), 3,4,7,8-tetramethyl-1,10-phenanthroline (99%, BLDPharm), 4,7-Dimethoxy-1,10-phenanthroline (97%, BLDPharm), tetra-*N*-butylammonium chloride (anhydrous, Fluorochem), perchloric acid (aq. solution, ~70%, Thermo Fisher Scientific), sodium tetrafluoroborate (>95%, TCI), sodium tetrakis[3,5-bis(trifluoromethyl)phenyl]borate (97%, Ark Pharm), silver nitrate (ACS reagent grade, Merck), silver trifluoromethane sulfonate (99%, Acros Organics) were purchased from commercial suppliers and used as received. 2,2'-Bipyrazine,[58] 4,4'-bistrifluoromethyl-2,2'-bipyridine,[59] 4,4',5,5'-tetramethyl-2,2'-bipyridine,[60] 1,4,5,8-tetraazaphenanthrene,[61,62] dipyrido[3,2-a:2',3'-c]phenazine,[63] and 4,4'-phenyl-2,2'-bipyridine,[64] were prepared following reported procedures. Water was purified by a Millipore Milli-Q system.

Nuclear Magnetic Resonance. ^{1}H-NMR spectroscopy was performed on a Bruker AC-300 Avance II (300 MHz) or a JEOL JNM-ECZL R (400 MHz and 600 MHz) at 293 K. The chemical shifts (in ppm) were measured versus the residual peak of the solvent as an internal standard.

High-Resolution Mass Spectrometry. High-resolution ESI-MS was performed with a Q-Extractive orbitrap from ThermoFisher using reserpine as the internal standard. Samples were ionized by electrospray ionization (ESI).

UV-Visible Absorption. UV−vis absorption spectra were recorded on an Agilent Cary 60 spectrophotometer in a quartz cuvette with a 1 cm path length. Molar absorption coefficients were determined in at least three independent measurements with a less than 5% standard deviation.

Time-Resolved and Steady-State Photoluminescence. Time-resolved and steady-state photoluminescence spectra were recorded on an FS5 Spectrofluorometer from Edinburgh Instruments equipped with a time-correlated single photon counting module. The steady-state photoluminescence spectra were recorded using a 150 W Xenon arc lamp as the excitation source. The photoluminescence was detected at a right angle to the excitation beam using a single photon counting PMT-900 in a temperature-stabilized housing. The spectra were integrated for 0.1–0.2 s at each wavelength, and three spectra were averaged. Steady-state photoluminescence spectra were corrected for the detector's response. For weakly emitting complexes, the emission spectra were corrected with a smooth function. For $[Os(dMeObpy)_3](PF_6)_2$, the emission was approximated by fitting with two Gaussian curves to estimate the emission outside of the detection window of the instrumental setup. Time-resolved photoluminescence data were collected on the FS5 using the time-correlated single photon counting technique (TCSPC). Excitation was achieved with a 510 ± 5 nm diode laser (Edinburgh Instruments EPL-510, 90 ps pulse width at 10 MHz) for osmium

complexes and a 450 ± 5 nm diode laser (EPL-450, 85 ps pulse width at 10 MHz) for ruthenium complexes. Photons reaching the detector were accumulated to reach a count of 10,000.

Variable Temperature Measurements. Variable temperature measurements were obtained using the time-correlated single photon counting technique on the Edinburgh Instruments FS5 Spectrofluorometer described above mounted with a liquid nitrogen CoolSpeK UV USP-203 four-window cryostat from Unisoku. 77K measurements were performed using the steady-state photoluminescence mode of the FS5 Spectrofluorometer.

Electrochemistry. Cyclic voltammetry was performed with an Autolab PGSTAT 100 potentiostat using a standard three-electrode-cell, i.e., a glassy carbon disk working electrode (approximate area = 3 mm^2), a platinum wire counter electrode, and an aqueous Ag/AgCl reference electrode (salt bridge: 3 M KCl/saturated AgCl). Experiments were performed in dry acetonitrile with 0.1 M $TBAPF_6$ as electrolyte at a scan rate of 0.1 to 0.3 V s^{-1}. The sample, with a complex concentration of 1 mM, was purged with argon before the measurement. For comparison purposes, the electrochemical potentials were converted to SCE by subtracting 0.036 V.

Experimental Procedures

Caution: Most reactions were carried out in an ACE pressure tube that was heated behind an explosion shield for increased safety. Some procedures deal with handling OsO_4, perchloric acid, and the isolation of perchlorate salts. Additional protective equipment was used when handling OsO_4 (double glove and avoiding any skin exposure), and any object in contact with OsO_4 was soaked for 2 hours in a 1M sodium sulfite solution. Perchloric acid was used in a regular fumehood, but some universities recommend fumehood specific for perchloric acid handling. Although we did not experience any issues, perchlorate salts can be potentially explosive, so they must be handled with care.

Synthesis of Ru(II) photosensitizers

General Procedure for the Synthesis of $[Ru(L)_3](PF_6)_2$. $RuCl_3.3H_2O$ (500 mg, 1.91 mmol, 1.0 eq.) and the desired ligand (6.69 mmol, 3.5 eq.) were placed in a 100 mL ACE sealed tube that contained a magnetic stirrer. Ethylene glycol (30 mL) was added, and the mixture was purged with argon for 15 minutes. The tube was then sealed under argon and stirred at 180 °C for 16 hours, unless otherwise specified. The reaction was kept in the dark and carried out behind an explosion shield. After reaction, the mixture was allowed to cool to room temperature and diluted with milliQ water (30 mL). Ammonium hexafluorophosphate (1.9 g, 6 eq.) was then gradually added under stirring, which induced the precipitation of the desired complex. The precipitate was collected by filtration and washed with copious amounts of milliQ water. The isolated complex was redissolved in acetonitrile and the solution was then slowly added to a stirred solution of diethyl ether to induce precipitation. The solid was collected by filtration, washed with diethyl ether, and dried in a vacuum desiccator for 24 hours. If needed, the photosensitizer was further purified.

$[Ru(bpy)_3](PF_6)_2$. Synthesized using the general procedure for ruthenium complexes. The crude product was dissolved in 20 mL of acetonitrile during workup and precipitated in 100 mL of diethyl ether. No additional purification was needed, affording the complex as an orange powder (1.57 g, 1.83 mmol, 95% yield). ^{1}H NMR (400 MHz, CD_3CN) δ 8.49 (d, *J* = 8.2 Hz, 6H), 8.05 (td, *J* = 7.9, 1.5 Hz, 6H), 7.80 – 7.66 (m, 6H), 7.39 (ddd, *J* = 7.7, 5.6, 1.3 Hz, 6H) ppm. NMR shifts match those reported in the literature.[65]

$[Ru(phen)_3](PF_6)_2$. Synthesized using the general procedure for ruthenium complexes. The crude product was dissolved in 15 mL of acetonitrile during workup and precipitated in 150 mL of diethyl ether. No additional purification was needed, affording the complex as an orange powder (1.67 g, 1.84 mmol, 94% yield). ^{1}H-NMR (600 MHz, CD_3CN) δ 8.59 (dd, *J* = 8.3, 1.2 Hz, 6H), 8.24 (s, 6H), 8.01 (dd, *J* = 5.2, 1.3 Hz, 6H), 7.61 (dd, *J* = 8.3, 5.3 Hz, 6H) ppm. NMR shifts match those reported in the literature.[57]

$[Ru(Bphen)_3](PF_6)_2$. Synthesized using a modified procedure. $RuCl_3.3H_2O$ (52 mg, 200 μmol, 1.0 eq.) and bathophenanthroline (219 mg, 660 μmol, 3.3 eq.) were placed in a 50 mL ACE sealed tube that contained a magnetic stirrer. Ethylene glycol (15 mL) was added, and the mixture was purged with argon for 15 minutes. The tube was then sealed under argon and stirred at 180 °C for 16 hours. The reaction was kept in the dark and carried out behind an explosion shield. After the reaction, the mixture was brought to room temperature. diluted with Milli-Q water (30 mL) and ammonium hexafluorophosphate (195 mg, 6 eq.) was gradually added under stirring, which induced the precipitation of the desired complex. The precipitate was collected by filtration and washed with copious amounts of water and diethyl ether. The crude product was purified by column chromatography (SiO_2, CH_2Cl_2/MeOH 95:5). The solvents were removed, affording the complex as a red powder (240 mg, 568 μmol, 86% yield) after drying *in-vacuo*. ^{1}H-NMR (600 MHz, CD_3CN) δ 8.28 (d, *J* = 5.5 Hz, 6H), 8.22 (s, 6H), 7.66 (d, *J* = 5.5 Hz, 6H), 7.64 – 7.60 (m, 30H) ppm. NMR shifts match those reported in the literature.[66]

$[Ru(bpz)_3](PF_6)_2$. Synthesized using the general procedure for ruthenium complexes. The crude product was dissolved in 150 mL of acetonitrile during workup and precipitated in 750 mL of diethyl ether. No additional purification was needed, affording the complex as a brown powder (1.32 g, 1.53 mmol, 80% yield). ^{1}H NMR (400 MHz, CD_3CN) δ 9.78 (s, 6H), 8.64 (d, *J* = 3.3 Hz, 6H), 7.83 (d, *J* = 3.3 Hz, 6H) ppm. NMR shifts match those reported in the literature.[67]

$[Ru(TAP)_3](PF_6)_2$. Synthesized using the general procedure for ruthenium complexes. The crude product was dissolved in 20 mL of acetonitrile during workup and precipitated in 200 mL of diethyl ether. This procedure was repeated three times. No additional purification was needed, affording the complex as a pale brown powder (600 mg, 640 μmol, 33% yield). ^{1}H-NMR (600 MHz, CD_3CN) δ 8.99 (d, *J* = 2.7 Hz, 6H), 8.63 (s, 6H), 8.24 (d, *J* = 2.7 Hz, 6H) ppm. NMR shifts match those reported in the literature.[68]

$[Ru(^{dtBu}bpy)_3](PF_6)_2$. Synthesized using the general procedure for ruthenium complexes. During workup, the crude product was dissolved in 20 mL of acetonitrile and precipitated in 350 mL of diethyl ether. No additional purification was needed, affording the complex as an orange powder (2.20 g, 1.84 mmol, 96% yield). ^{1}H-NMR (300 MHz, CD_3CN) δ 8.46 (d, *J* = 2.0 Hz, 6H), 7.55 (d, *J* = 6.0 Hz, 6H), 7.39 (dd, *J* = 6.1, 2.1 Hz, 6H), 1.40 (s, 54H) ppm. NMR shifts match those reported in the literature.[69]

$[Ru(^{tMe}bpy)_3](PF_6)_2$. Synthesized using the modified general procedure for ruthenium complexes on a different scale. $RuCl_3.3H_2O$ (177 mg, 670 μmol, 1.0 eq.) and ^{tMe}bpy ligand (474 mg, 2.23 mmol, 3.3 eq.) were placed in a 100 mL ACE sealed tube that was equipped with a magnetic stirrer. Ethylene glycol (15 mL) was added, and the mixture was purged with argon for 15 minutes. The tube was then sealed under argon and stirred at

180 °C for 16 hours. The reaction was kept in the dark and carried out behind an explosion shield. After reaction, the mixture was brought to room temperature and diluted with milliQ water (30 mL). Ammonium hexafluorophosphate (662 mg, 6 eq.) was then gradually added under stirring, which induced the precipitation of the desired complex. The precipitate was collected by filtration and washed with copious amounts of water and diethyl ether. The crude product was then purified by column chromatography (SiO_2, CH_2Cl_2/MeOH 98:2). The solvents were then evaporated, affording the complex as an orange powder (467 mg, 455 μmol, 68% yield). ^{1}H-NMR (600 MHz, CD_3CN) δ 8.20 (s, 6H), 7.29 (s, 6H), 2.43 (s, 18H), 2.07 (s, 18H) ppm. NMR shifts match those reported in the literature.[70]

[Ru($^{4,4'dMe}$bpy)$_3$](PF$_6$)$_2$. Synthesized using the general procedure for ruthenium complexes. During workup, the crude product was dissolved in 25 mL of acetonitrile and precipitated in 150 mL of diethyl ether. No additional purification was needed, affording the complex as an orange powder (1.73 g, 1.83 mmol, 96% yield). ^{1}H NMR (400 MHz, CD_3CN) δ 8.33 – 8.30 (m, 6H), 7.51 (d, *J* = 5.9 Hz, 6H), 7.20 (ddd, *J* = 5.9, 2.0, 0.9 Hz, 6H) ppm. NMR shifts match those reported in the literature.[69]

[Ru($^{5,5'dMe}$bpy)$_3$](PF$_6$)$_2$. Synthesized using the general procedure for ruthenium complexes. During workup, the crude product was dissolved in 25 mL of acetonitrile and precipitated in 250 mL of diethyl ether. No additional purification was needed, affording the complex as an orange powder (1.78 g, 1.89 mmol, 99% yield).). ^{1}H NMR (400 MHz, CD_3CN) δ 8.30 (d, *J* = 8.3 Hz, 6H), 7.85 – 7.78 (m, 6H), 7.46 – 7.39 (m, 6H), 2.19 (s, 18H) ppm. NMR shifts match those reported in the literature.[71]

[Ru(^{dnonyl}bpy)$_3$](PF$_6$)$_2$. Synthesized using the general procedure for ruthenium complexes with a modified workup protocol. After the reaction, the mixture was brought to room temperature and diluted with Milli-Q water (30 mL). Ammonium hexafluorophosphate (1.9 g, 6 eq.) was then gradually added under stirring, which induced the precipitation of the desired complex. The precipitate was collected by filtration and washed with copious amounts of water and *n*-hexane (as the complex was soluble in diethyl ether). The crude product was then purified by column chromatography (neutral Al_2O_3, CH_2Cl_2). The solvent was removed, affording the complex as a dark red powder (2.69 g, 1.66 mmol, 87% yield). ^{1}H-NMR (600 MHz, DMSO-d_6) δ 8.75 (s, 6H), 7.52 (d, *J* = 5.9 Hz, 6H), 7.36 (d, *J* = 5.9 Hz, 6H), 2.75 (t, *J* = 7.8 Hz, 12H), 1.64 (t, *J* = 7.7 Hz, 12H), 1.33 – 1.06 (m, 72H), 0.82 (t, *J* = 7.0 Hz, 18H) ppm. NMR shifts match those reported in the literature.[72]

[Ru(^{dMeO}bpy)$_3$](PF$_6$)$_2$. Synthesized using a modified literature procedure.[73] $RuCl_3.3H_2O$ (250 mg, 955 μmol, 1.0 eq.) and the ^{dMeO}bpy ligand (723 mg, 3.35 mmol, 3.5 eq.) were placed in a round bottom flask. A mixture of DMF/water/MeOH (1:1:1, 21 mL in total) was then added, and the solution purged with argon for 30 minutes and stirred at 140 °C for 60 hours. After the reaction, the mixture was brought to room temperature and diluted with Milli-Q water (30 mL). Ammonium hexafluorophosphate (0.95 g, 6 eq.) was then gradually added under stirring, which induced the precipitation of the desired complex. The precipitate was collected by filtration and washed with copious amounts of water and diethyl ether. The complex was then dissolved in acetonitrile (25 mL) and precipitated by addition to a stirred solution of diethyl ether (250 mL). No additional purification was needed, affording the complex as a dark red powder (926 mg, 891 μmol, 93% yield). ^{1}H-NMR (600 MHz, CD_3CN) δ 7.98 (d, *J* = 2.9 Hz, 6H), 7.52 (dd, *J* = 6.5, 1.2 Hz, 6H), 7.09 – 6.80 (m, 6H), 3.98 (s, 18H) ppm. NMR shifts match those reported in the literature.[69]

[Ru(^{dCF3}bpy)$_3$](PF$_6$)$_2$. Synthesized using the general procedure for ruthenium complexes. The crude product was dissolved in 40 mL of acetonitrile during workup and precipitated in 400 mL of diethyl ether. No additional purification was needed, affording the complex as an orange powder (2.05 g, 1.59 mmol, 83% yield). ^{1}H NMR (400 MHz, CD_3CN) δ 8.95 (s, 6H), 7.97 (d, *J* = 5.9 Hz, 6H), 7.72 (d, *J* = 6.0 Hz, 6H) ppm.

[Ru(^{dMeO}phen)$_3$](PF$_6$)$_2$. Synthesized using a modified procedure. $RuCl_3.3H_2O$ (130 mg, 500 μmol, 1.0 eq.) and ^{dMeO}Phen ligand (420 mg, 1.75 mmol, 3.5 eq.) were placed in a 50 mL ACE sealed tube equipped with a magnetic stirrer. A mixture of DMF/water/MeOH (1:1:1, 12 mL in total) was added, and the mixture was purged with argon for 20 minutes. The tube was then sealed under argon and stirred at 160 °C for 16 hours. The reaction was kept in the dark and carried out behind an explosion shield. After the reaction, the mixture was brought to room temperature and diluted with Milli-Q water (20 mL). Ammonium hexafluorophosphate (490 mg, 6 eq.) was then gradually added under stirring, which induced the precipitation of the desired complex. The orange precipitate was collected by filtration, redissolved in acetonitrile (10 mL), and precipitated by addition to a stirred solution of diethyl ether (250 mL). The crude product was then purified by column chromatography (neutral Al_2O_3, CH_2Cl_2/MeCN 9:1 → MeCN/MeOH 9:1). The solvents were then evaporated and the product recrystallized from ethanol, affording the complex as an orange powder (352 mg, 304 μmol, 61% yield). ^{1}H-NMR (400 MHz, CD_3CN) δ 8.34 (s, 6H), 7.86 (d, *J* = 6.2 Hz, 6H), 7.03 (d, *J* = 6.2 Hz, 6H), 4.10 (s, 18H) ppm. NMR shifts match those reported in the literature.[69]

[Ru(^{tMe}phen)$_3$](PF$_6$)$_2$. Synthesized using the modified general procedure for ruthenium complexes on a different scale. $RuCl_3.3H_2O$ (130 mg, 500 μmol, 1.0 eq.) and ^{tMe}Phen ligand (414 mg, 1.75 mmol, 3.5 eq.) were placed in a 50 mL ACE-sealed tube equipped with a magnetic stirrer. Ethylene glycol (8 mL) was added, and the mixture was purged with argon for 15 minutes. The tube was then sealed under argon and stirred at 180 °C for 16 hours. The reaction was kept in the dark and carried out behind an explosion shield. After the reaction, the mixture was brought to room temperature and diluted with Milli-Q water (20 mL). Ammonium hexafluorophosphate (490 mg, 6 eq.) was then gradually added under stirring, which induced the precipitation of the desired complex. The precipitate was collected by filtration, redissolved in acetonitrile (50 mL), and precipitated by addition to a stirred solution of diethyl ether (300 mL). The crude product was then purified by column chromatography (neutral Al_2O_3, CH_2Cl_2 → CH_2Cl_2/MeCN 20:1). The solvents were then evaporated, affording the complex as an orange powder (121 mg, 106 μmol, 21% yield). ^{1}H-NMR (400 MHz, CD_3CN) δ 8.35 (s, 6H), 7.65 (s, 6H), 2.76 (s, 18H), 2.20 (s, 18H) ppm. NMR shifts match those reported in the literature.[74]

[Ru(dppz)$_3$](PF$_6$)$_2$. Synthesized using a modified procedure. $RuCl_3.3H_2O$ (55.9 mg, 214 μmol, 1.0 eq.) and dppz (200 mg, 708 μmol, 3.3 eq.) were placed in a 50 mL ACE sealed tube with a magnetic stirrer. Ethylene glycol (3 mL) was added, and the mixture was purged with argon for 15 minutes. The tube was then sealed under argon and stirred at 180 °C for 16 hours. The reaction was kept in the dark and carried out behind an explosion shield. After the reaction, the mixture was brought to room temperature and diluted with ethanol (10 mL). The mixture was

then poured on 200 mL of diethyl ether, and the precipitate was collected by filtration and washed with diethyl ether. The precipitate was loaded on an LH20 size exclusion chromatography column and eluted with methanol. The desired orange fraction was collected and evaporated under reduced pressure to yield the title compound as a chloride salt. The photosensitizer could be isolated as PF_6 by performing ion metathesis using a saturated solution of ammonium hexafluorophosphate. The precipitate was collected by filtration and washed with copious amounts of water and diethyl ether affording the title compound as an orange powder (67 mg, 54 μmol, 25% yield). ^{1}H NMR (400 MHz, CD_3CN) δ 9.69 (s, 6H), 8.50 (dd, *J* = 6.7, 3.5 Hz, 6H), 8.31 (d, *J* = 5.4 Hz, 6H), 8.16 (dd, *J* = 6.9 Hz, *J* = 3.2 Hz, 6H), 7.84 (dd, *J* = 8.2, 5.4 Hz, 6H) ppm. NMR shifts match those reported in the literature.[75]

[Ru(Bbpy)$_3$](PF$_6$)$_2$. Synthesized using a modified procedure. $RuCl_3.3H_2O$ (52.0 mg, 199 μmol, 1.0 eq.) and Bbpy (200 mg, 649 μmol, 3.3 eq.) were placed in a 100 mL ACE-sealed tube equipped with a magnetic stirrer. Ethylene glycol (3 mL) was added, and the mixture was purged with argon for 15 minutes. The tube was then sealed under argon and stirred at 180 °C for 16 hours. The reaction was kept in the dark and carried out behind an explosion shield. After the reaction, the mixture was brought to room temperature and diluted with ethanol (10 mL). The mixture was then poured on 500 mL of diethyl ether, and the precipitate was collected by filtration and washed with diethyl ether. The precipitate was loaded on an LH20 size exclusion chromatography column and eluted with methanol. The desired orange fraction was collected and evaporated under reduced pressure to yield the title compound as a chloride salt. The photosensitizer could be isolated as PF_6 by performing ion metathesis using a saturated solution of ammonium hexafluorophosphate. The precipitate was collected by filtration and washed with copious amounts of water and diethyl ether affording the title compound as an crystalline dark red powder (136 mg, 132 μmol, 66% yield). ^{1}H NMR (400 MHz, CD_3CN) δ 8.97 (d, *J* = 1.7 Hz, 6H), 8.03 – 7.87 (m, 18H), 7.72 (dd, *J* = 6.0, 1.9 Hz, 6H), 7.66 – 7.45 (m, 18H) ppm. NMR shifts match those reported in the literature.[76]

Synthesis of Os(II) photosensitizers

[OsCl$_6$](NH$_4$)$_2$. Ammonium hexachloroosmate ([$OsCl_6$](NH_4)$_2$) was prepared following a slightly modified procedure originally reported by Dwyer and Hogarth.[77] Osmium tetroxide (10.0 g, 39.3 mmol, 1.0 eq.) was dissolved in concentrated aq. HCl (37%, 300 mL) containing iron(II) chloride tetrahydrate (85.0 g, 428 mmol, 10.9 eq.). The mixture was stirred at 100 °C for 2 hours, followed by the addition of an aqueous NH_4Cl solution (20%, 10 mL). The mixture was allowed to cool to room temperature and was then cooled at 0 °C in an ice bath. The red crystalline precipitate was collected by filtration, washed with copious amount of ethanol/water (8:2) and absolute ethanol. The final product was isolated and was further dried under vacuum to obtain a red crystalline powder (15.9 g, 36.2 mmol, 92%).

General Procedure for the synthesis of [Os(L)$_3$](PF$_6$)$_2$.

[$OsCl_6$](NH_4)$_2$ (850 mg, 1.94 mmol, 1.0 eq.) and the desired ligand (6.78 mmol, 3.5 eq.) were placed in a 100 mL ACE-sealed tube that contained a magnetic stirrer. Ethylene glycol (30 mL) was added, and the mixture was purged with argon for 15 minutes. The tube was then sealed under argon and stirred at 230 °C for 48 hours unless otherwise specified. The reaction was kept in the dark and carried out behind an explosion shield. After the reaction, the mixture was brought to room temperature and diluted with Milli-Q water (30 mL). Ammonium hexafluorophosphate (1.9 g, 6 eq.) was then gradually added under stirring unless otherwise specified, which induced the precipitation of the desired complex. The precipitate was collected by filtration and washed with copious amounts of Milli-Q water. The isolated complex was redissolved in acetonitrile, and the solution was then slowly added to a stirred solution of diethyl ether to induce precipitation. The solid was collected by filtration, washed with diethyl ether, and dried in a vacuum desiccator for 24 hours. If needed, the photosensitizer was further purified.

[Os(bpy)$_3$](PF$_6$)$_2$. Synthesized using the general procedure for osmium complexes. The crude product was dissolved in 50 mL of acetonitrile during workup and precipitated in 500 mL of diethyl ether. No additional purification was needed, affording the complex as a dark green powder (1.67 g, 1.76 mmol, 91% yield). ^{1}H NMR (400 MHz, CD_3CN) δ 8.47 (dd, *J* = 8.2, 1.1 Hz, 6H), 7.93 – 7.79 (m, 6H), 7.63 (dd, *J* = 5.7, 1.0 Hz, 6H), 7.30 (ddt, *J* = 7.0 Hz, *J* = 5.7 Hz, *J* = 1.3 Hz, 6H) ppm. NMR shifts match those reported in the literature.[73]

[Os(phen)$_3$](PF$_6$)$_2$. Synthesized using the general procedure for osmium complexes with a modified workup protocol. The reaction mixture was diluted with 30 mL of absolute ethanol, and the complex was precipitated from ethylene glycol with 400 mL of diethyl ether. The crude product was then purified by column chromatography (Al_2O_3, CH_3CN→ CH_3CN/H_2O 9:1). The solvents were removed, the complex dissolved in water (40 mL) and precipitated by the addition of ammonium hexafluorophosphate (1.9 g, 6 eq.). The precipitate was collected by filtration and washed with copious amounts of water and diethyl ether, affording the complex as a black powder (840 mg, 820 μmol, 42% yield). ^{1}H-NMR (300 MHz, CD_3CN) δ 8.37 (dd, *J* = 8.2, 1.2 Hz, 6H), 8.23 (s, 6H), 7.92 (dd, *J* = 5.4, 1.2 Hz, 6H), 7.54 (dd, *J* = 8.3, 5.4 Hz, 6H) ppm. NMR shifts match those reported in the literature.[73]

[Os(Bphen)$_3$](PF$_6$)$_2$. Synthesized using a modified procedure. [$OsCl_6$](NH_4)$_2$ (303 mg, 690 μmol, 1.0 eq.) and the bathophenanthroline ligand (757 mg, 2.27 mmol, 3.3 eq.) were placed in a 100 mL ACE sealed tube that contained a magnetic stirrer. Ethylene glycol (15 mL) was added, and the mixture was purged with argon for 15 minutes. The tube was then sealed under argon and stirred at 230 °C for 48 hours. The reaction was kept in the dark and carried out behind an explosion shield. After the reaction, the mixture was brought to room temperature and diluted with Milli-Q water (30 mL). Ammonium hexafluorophosphate (675 mg, 6 eq.) was then gradually added under stirring unless otherwise specified, which induced the precipitation of the desired complex. The precipitate was collected by filtration and washed with copious amounts of water and diethyl ether. The crude product was then purified by column chromatography (SiO_2, CH_2Cl_2/MeOH 85:15). The solvents were removed, affording the complex as a dark brown powder (742 mg, 505 μmol, 73% yield). ^{1}H-NMR (600 MHz, CD_3CN) δ 8.23 (s, 6H), 8.19 (d, *J* = 5.7 Hz, 6H), 7.67 – 7.60 (m, 30H), 7.59 (d, *J* = 5.5 Hz, 6H) ppm. NMR shifts match those reported in the literature.[78]

[Os(bpz)$_3$](PF$_6$)$_2$. Synthesized using a modified workup procedure and with a modified scale, i.e. [$OsCl_6$](NH_4)$_2$ (658 mg, 1.50 mmol, 1.0 eq.) and the 2,2'-bipyrazine ligand (830 mg, 5.25 mmol, 3.5 eq.) in ethylene glycol (25 mL). The reaction mixture was diluted with water (50 mL) and filtered to remove insoluble materials. The mixture was then purified by anion exchange chromatography (Sephadex C-25, NaCl aqueous solution (0.05 to

0.20 M)). The solvent was then removed, and the complex dissolved in a minimal amount of methanol and filtered to remove NaCl, this operation was repeated 5 times. The dark solid was dissolved in water and precipitated by the addition of sodium hexafluorophosphate (1.5 g, 6.0 eq.). The precipitate was collected by filtration and washed with water and diethyl ether, affording the complex as a dark green powder (42 mg, 44 μmol, 3% yield). ^{1}H-NMR (600 MHz, CD_3CN) δ 9.76 (d, *J* = 1.3 Hz, 6H), 8.50 (d, *J* = 3.3 Hz, 6H), 7.74 (dd, *J* = 3.3, 1.2 Hz, 6H) ppm. NMR shifts match those reported in the literature.[73]

[Os(TAP)$_3$](PF$_6$)$_2$. Synthesized using a modified workup procedure and with a modified scale. The reaction was performed starting with $[OsCl_6](NH_4)_2$ (658 mg, 1.50 mmol, 1.0 eq.) and the 1,4,5,8-tetraazaphenanthrene ligand (956 mg, 5.25 mmol, 3.5 eq.) in ethylene glycol (25 mL). The reaction mixture was diluted with water (50 mL) and filtered to remove insoluble materials. The mixture was then purified by anion exchange chromatography (Sephadex C-25, NaCl aqueous solution (0.05 to 0.20 M)). The solvents were then evaporated, and the complex dissolved in a minimal amount of methanol and filtered to remove NaCl, this operation was repeated 3 to 5 times. The dark solid was dissolved in water and precipitated by the addition of sodium hexafluorophosphate (1.5 g, 6 eq.). The precipitate was collected by filtration and washed with water and diethyl ether, affording the complex as a dark brown powder (315 mg, 294 μmol, 20% yield). ^{1}H-NMR (600 MHz, CD_3CN) δ 8.86 (d, *J* = 2.9 Hz, 6H), 8.63 (s, 6H), 8.18 (d, *J* = 2.9 Hz, 6H) ppm. NMR shifts match those reported in the literature.[79]

A two-step procedure was also attempted for the synthesis of $[Os(TAP)_3]^{2+}$. The reaction started with $[OsCl_6](NH_4)_2$ (120 mg, 0.27 mmol, 1.0 eq.) and 1,4,5,8-tetraazaphenanthrene (100 mg, 0.55 mmol, 2.0 eq.) placed in ethylene glycol (4.8 mL) and refluxed at 200 °C under Argon for 1 hour. After the reaction was cooled down to room temperature, a reduction with 1M $Na_2S_2O_4$ (12 ml) was performed. The precipitate was collected by centrifugation and washed with water, cold ethanol, and diethyl ether. $[Os(TAP)_2Cl_2]$ was recovered as a dark black-purple powder (115 mg, 180 μmol, 67% yield) and used without further purification. $[Os(TAP)_2Cl_2]$ (50 mg, 0.16 mmol, 1.0 eq) and 1,4,5,8-tetraazaphenanthrene (16 mg, 0.16 mmol, 1.0 eq.) were placed in ethylene glycol (15 mL) under Argon and the reaction media was heated in the microwave at 180°C for 2.5 hours. Then, a precipitation was followed with ethanol and diethyl ether. The residue was dissolved in methanol and filtered on 0.2 μm syringe filter. The final product (44 mg, 49 μmol, 32% yield) was collected by using a size exclusion chromatography LH20 with MeOH as eluent.

[Os(^{dtBu}bpy)$_3$](PF$_6$)$_2$. Synthesized using a modified workup procedure. The complex was dissolved in 30 mL of acetone and precipitated in 400 mL of diethyl ether. Further purification was performed by column chromatography (Al_2O_3, CH_3CN/H_2O 100:0 to 95:5). Removing the solvents afforded the complex as a dark green powder (2.12 g, 1.65 mmol, 85% yield). ^{1}H-NMR (300 MHz, CD_3CN) δ 8.43 (d, *J* = 1.5 Hz, 6H), 7.46 (dd, *J* = 6.2, 0.7 Hz, 6H), 7.30 (dd, *J* = 6.2, 2.1 Hz, 6H), 1.40 (s, 54H) ppm. NMR shifts match those reported in the literature.[73]

[Os(^{tMe}bpy)$_3$](PF$_6$)$_2$. Synthesized using a modified procedure. $[OsCl_6](NH_4)_2$ (303 mg, 690 μmol, 1.0 eq.) and the ^{tMe}bpy ligand (483 mg, 2.27 mmol, 3.3 eq.) were placed in a 100 mL ACE sealed tube that contained a magnetic stirrer. Ethylene glycol (15 mL) was added, and the mixture was purged with argon for 15 minutes. The tube was then sealed under argon and stirred at 230 °C for 48 hours. The reaction kept in the dark and carried out behind an explosion shield. After reaction, the mixture was brought to room temperature and diluted with milliQ water (20 mL). Ammonium hexafluorophosphate (675 mg, 6 eq.) was then gradually added under stirring which induced the precipitation of the desired complex. The precipitate was collected by filtration and washed with copious amounts of water and diethyl ether. The crude product was then purified by column chromatography (SiO_2, CH_2Cl_2/MeOH 95:5). The solvents were then evaporated, affording the complex as dark brown powder (412 mg, 370 μmol, 54% yield). ^{1}H-NMR (600 MHz, CD_3CN) δ 8.17 (s, 6H), 7.19 (s, 6H), 2.49 (s, 18H), 2.08 (s, 18H) ppm. High resolution ESI-MS m/z calculated for $[C_{42}H_{48}N_6{}^{184}Os]^{2+}$ = 410.17272; found 410.17351.

[Os($^{4,4'dMe}$bpy)$_3$](PF$_6$)$_2$. Synthesized using the general procedure for osmium complexes. During workup, the crude product was dissolved in 90 mL of acetonitrile and precipitated in 900 mL of diethyl ether. No additional purification was needed, affording the complex as a dark green powder (1.76 g, 1.70 mmol, 88% yield). ^{1}H NMR (400 MHz, CD_3CN) δ 8.28 (s, 6H), 7.42 (d, *J* = 6.0 Hz, 6H), 7.11 (d, *J* = 5.9 Hz, 6H), 2.58 (s, 18H) ppm NMR shifts match those reported in the literature.[73]

[Os($^{5,5'dMe}$bpy)$_3$](PF$_6$)$_2$. Synthesized using the general procedure for osmium complexes. The crude product was dissolved in 70 mL of acetonitrile during workup and precipitated in 700 mL of diethyl ether. No additional purification was needed, affording the complex as a dark green powder (1.82 g, 1.76 mmol, 91% yield). ^{1}H NMR (400 MHz, CD_3CN) δ 8.28 (d, *J* = 8.4 Hz, 6H), 7.66 (d, *J* = 8.3 Hz, 6H), 7.33 (s, 6H), 2.19 (s, 18H) ppm. NMR shifts match those reported in the literature.[73]

[Os(^{dnonyl}bpy)$_3$](PF$_6$)$_2$. Synthesized using the general procedure for osmium complexes with a modified workup protocol. After the reaction, the mixture was brought to room temperature and diluted with milliQ water (30 mL). Ammonium hexafluorophosphate (1.9 g, 6 eq.) was then gradually added under stirring, which induced the precipitation of the desired complex. The precipitate was collected by filtration and washed with copious amounts of water and *n*-hexane (as the complex was soluble in diethyl ether). The crude product was then purified by column chromatography (neutral Al_2O_3, CH_2Cl_2). The solvent was then removed, affording the complex as a dark green powder (1.57 g, 920 μmol, 48% yield). ^{1}H NMR (400 MHz, DMSO-d_6) δ 8.73 – 8.64 (m, 6H), 7.43 (d, *J* = 6.0 Hz, 6H), 7.27 (dd, *J* = 6.0, 1.9 Hz, 6H), 2.80 (t, *J* = 7.7 Hz, 12H), 1.63 (m, 12H), 1.34 – 1.11 (m, 72H), 0.93 – 0.71 (m, 18H) ppm. NMR shifts match those reported in the literature.[80]

[Os(^{dMeO}bpy)$_3$](PF$_6$)$_2$. Synthesized using a modified procedure.[73] $[OsCl_6](NH_4)_2$ (445 mg, 1.01 mmol, 1.0 eq.) and the ^{dMeO}bpy ligand (767 mg, 3.55 mmol, 3.5 eq.) were placed in a round bottom flask. A mixture of DMF/water/MeOH (1:1:1, 21 mL in total) was then added, and the solution was purged with argon for 30 minutes and then stirred at 140 °C for 60 hours. After the reaction, the mixture was brought to room temperature and diluted with milliQ water (30 mL). Ammonium hexafluorophosphate (950 mg, 6 eq.) was then gradually added under stirring, which induced the precipitation of the desired complex. The precipitate was collected by filtration and washed with copious amounts of water and diethyl ether. The crude product was purified by column chromatography (neutral Al_2O_3, CH3CN), and the solvent was then removed, affording the complex as a dark brown powder (630 mg, 560 μmol, 55% yield). ^{1}H-NMR (600 MHz, CD_3CN) δ 7.95 (d, *J* = 2.7 Hz, 6H), 7.43 (d, *J* = 6.8 Hz, 6H), 6.88 (dd, *J* =

6.6 Hz, *J* = 2.7 Hz, 6H), 3.99 (s, 18H) ppm. NMR shifts match those reported in the literature.[73]

[Os(^{dCF3}bpy)$_3$](PF$_6$)$_2$. Synthesized using the general procedure for osmium complexes. During workup, the crude product was dissolved in 70 mL of acetonitrile and precipitated in 700 mL of diethyl ether. No additional purification was needed, affording the complex as a dark green powder (1.43 g, 1.04 mmol, 54% yield). ^{1}H-NMR (300 MHz, CD_3CN) δ 8.99 (s, 6H), 7.89 (d, *J* = 5.9 Hz, 6H), 7.61 (d, *J* = 5.3 Hz, 6H) ppm. High Resolution ESI-MS m/z calculated for $[C_{36}H_{18}N_{10}F_{18}{}^{184}Os]^{2+}$ = 530.04097; found 530.04210.

[Os(^{dMeO}phen)$_3$](PF$_6$)$_2$.

Synthesized using a modified procedure for osmium complexes on a different scale. $[OsCl_6](NH_4)_2$ (228 mg, 500 μmol, 1.0 eq.) and ^{dMeO}Phen ligand (420 mg, 1.75 mmol, 3.5 eq.) were placed in a 50 mL ACE sealed tube that was equipped with a magnetic stirrer. A mixture of DMF/water/MeOH (1:1:1, 12 mL in total) was added, and the mixture was purged with argon for 20 minutes. The tube was sealed under argon and stirred at 160 °C for 96 hours. The reaction was kept in the dark and carried out behind an explosion shield. After the reaction, the mixture was brought to room temperature and diluted with milliQ water (10 mL). Ammonium hexafluorophosphate (490 mg, 6 eq.) was then gradually added under stirring, which induced the precipitation of the desired complex. The black precipitate was collected by filtration, redissolved in acetonitrile (20 mL), and precipitated by addition to a stirred solution of diethyl ether (300 mL). The crude product was then purified by column chromatography (SiO_2, MeCN → MeCN/water/sat.aq. KNO_3 20:1:1). The solvents were then evaporated, and the complex redissolved in water (5 mL) and precipitated by the addition of saturated aqueous ammonium hexafluorophosphate. The complex was washed with copious amounts of water and diethyl ether and dried, affording the complex as a dark black powder (151 mg, 121μmol, 24% yield). ^{1}H NMR (400 MHz, CD_3CN) δ 8.33 (s, 3H), 7.77 (d, *J* = 6.2 Hz, 6H), 6.99 (d, *J* = 6.3 Hz, 6H), 4.10 (s, 18H) ppm ppm. NMR shifts match those reported in the literature.[73]

[Os(^{tMe}phen)$_3$](PF$_6$)$_2$. Synthesized using the modified general procedure for osmium complexes on a different scale. $OsCl_6](NH_4)_2$ (228 mg, 500 μmol, 1.0 eq.) and ^{tMe}Phen ligand (414 mg, 1.75 mmol, 3.5 eq.) were placed in a 50 mL ACE sealed tube that was equipped with a magnetic stirrer. Ethylene glycol (8 mL) was added, and the mixture was purged with argon for 15 minutes. The tube was then sealed under argon and stirred at 180 °C for 48 hours. The reaction was kept in the dark and carried out behind an explosion shield. After the reaction, the mixture was brought to room temperature and diluted with milliQ water (20 mL). Aqueous saturated potassium hexafluorophosphate solution was then gradually added under stirring, which induced the precipitation of the desired complex. The precipitate was collected by filtration, redissolved in acetonitrile (50 mL), and precipitated by addition to a stirred solution of diethyl ether (600 mL). The crude product was then purified by column chromatography (SiO_2, CH_2Cl_2→ CH_2Cl_2/MeCN 20:1). The solvents were then evaporated, affording the complex as a dark black powder (232 mg, 186 μmol, 37% yield). ^{1}H NMR (400 MHz, CD_3CN) δ 8.34 (s, 6H), 7.56 (s, 6H), 2.84 (s, 18H), 2.19 (s, 18H) ppm. NMR shifts match those reported in the literature.[73]

[Os(dppz)$_3$](PF$_6$)$_2$ Synthesized using a modified procedure. $[OsCl_6](NH_4)_2$ (88 mg, 200 μmol, 1.0 eq.) and dppz (200 mg, 708 μmol, 3.3 eq.) were placed in a 100 mL ACE sealed tube that was equipped with a magnetic stirrer. Ethylene glycol (3 mL) was added, and the mixture was purged with argon for 15 minutes. The tube was then sealed under argon and stirred at 230 °C for 48 hours. The reaction was kept in the dark and carried out behind an explosion shield. After the reaction, the mixture was brought to room temperature and diluted with ethanol (10 mL). The mixture was then poured on 200 mL of diethyl ether, and the precipitate was collected by filtration and washed with diethyl ether. The precipitate was loaded on an LH20 size exclusion chromatography column and eluted with methanol. The desired orange fraction was collected and evaporated under reduced pressure to yield the title compound as a chloride salt. The photosensitizer could be isolated as PF_6 by performing ion metathesis using a saturated solution of ammonium hexafluorophosphate. The precipitate was collected by filtration and washed with copious amounts of water and diethyl ether and recrystallized from ethanol affording the title compound as a dark green powder (24 mg, 18 μmol, 9% yield). ^{1}H NMR (400 MHz, CD_3CN) δ 9.49 (dd, *J* = 8.2, 1.2 Hz, 6H), 8.50 (dd, *J* = 6.5, 3.5 Hz, 6H), 8.27 – 8.21 (m, 6H), 8.16 (dd, *J* = 6.6, 3.4 Hz, 6H), 7.76 (dd, *J* = 8.2, 5.5 Hz, 6H) ppm.

[Os(Bbpy)$_3$](PF$_6$)$_2$. Synthesized using a modified procedure. $[OsCl_6](NH_4)_2$ (79 mg, 180 μmol, 1.0 eq.) and Bbpy (200 mg, 649 μmol, 3.6 eq.) were placed in a 100 mL ACE sealed tube that was equipped with a magnetic stirrer. Ethylene glycol (3 mL) was added, and the mixture was purged with argon for 15 minutes. The tube was then sealed under argon and stirred at 230 °C for 48 hours. The reaction was kept in the dark and carried out behind an explosion shield. After the reaction, the mixture was brought to room temperature and diluted with ethanol (10 mL). The mixture was then poured on 200 mL of diethyl ether, and the precipitate was collected by filtration and washed with diethyl ether. The precipitate was loaded on an LH20 size exclusion chromatography column and eluted with methanol. The desired orange fraction was collected and evaporated under reduced pressure to yield the title compound as a chloride salt. The photosensitizer could be isolated as PF_6 by performing ion metathesis using a saturated solution of ammonium hexafluorophosphate. The precipitate was collected by filtration and washed with copious amounts of water and diethyl ether affording the title compound as a dark green powder (123 mg, 110 μmol, 55 % yield).^{1}H NMR (400 MHz, CD_3CN) δ 8.92 (s, 6H), 7.91 (d, *J* = 7.4 Hz, 12H), 7.81 (d, *J* = 5.5 Hz, 6H), 7.61 – 7.46 (m, 24H) ppm.

Counter-Ion Exchange: The procedure for counter-ion exchange is described for $[Ru(bpy)_3]^{2+}$ but was also performed on $[Ru(^{dCF3}bpy)_3]^{2+}$, $[Ru(^{4,4'dMe}bpy)_3]^{2+}$, $[Os(bpy)_3]^{2+}$, $[Os(^{4,4'dMe}bpy)_3]^{2+}$ and $[Os(^{dCF3}bpy)_3]^{2+}$. The yields of these exchanges are tabulated in Table S1 together with additional experimental details.

[Ru(bpy)$_3$](Cl)$_2$. $[Ru(bpy)_3](PF_6)_2$ (200 mg, 233 mmol, 1.0 eq.) was dissolved in acetone (20 mL). Tetra-*n*-butylammonium chloride (TBACl, 408 mg, 1.47 mmol, 6.0 eq.) was then added under stirring, and an orange precipitate immediately appeared. The precipitate was then filtered, washed with acetone, and dried under vacuum to afford the desired product in a quantitative yield.

[Ru(bpy)$_3$](ClO$_4$)$_2$. $[Ru(bpy)_3](Cl)_2.6H_2O$ (200 mg, 267 mmol, 1.0 eq.) was dissolved in Milli-Q water (20 mL). A concentrated solution of $HClO_4$ (aq. solution, ~70%, less than 1 mL) was then added dropwise with a Pasteur pipette under stirring until no more solid formation was observed. The precipitate was then filtered and washed with cold ethanol and diethyl ether. The precipitate

was finally dried under vacuum to afford the desired product as an orange powder (187 mg, 243 μmol, 91% yield). The product is slightly soluble in water.

$[Ru(bpy)_3](BF_4)_2$. $[Ru(bpy)_3](Cl)_2.6H_2O$ (200 mg, 267 mmol, 1.0 eq.) was dissolved in Milli-Q water (20 mL). Sodium tetrafluoroborate ($NaBF_4$, 500 mg, 4.55 mmol, 17 eq.) was then added, and the mixture was stirred for 5 minutes before being cooled in the fridge at 4 °C for 10 minutes. The precipitate was filtered and washed with cold ethanol and diethyl ether. The precipitate was then dried under vacuum to afford the desired product as an orange powder (160 mg, 215 mmol, 81% yield). The product is slightly soluble in water and ethanol.

$[Ru(bpy)_3](BAr^F)_2$. $[Ru(bpy)_3](Cl)_2.6H_2O$ (200 mg, 267 μmol, 1.0 eq.) was dissolved in Milli-Q water (20 mL). A solution of sodium tetrakis[3,5-bis(trifluoromethyl)phenyl]borate ($NaBAr^F$, 567 mg, 640 mmol, 2.4 eq.) in methanol (5 mL) was added dropwise under stirring. The mixture was stirred for 10 minutes, and the precipitate was then filtered, washed with water, and dried under a vacuum. The solid was then dissolved in a minimum amount of dichloromethane and acetonitrile (CH_2Cl_2/CH_3CN 1:1) and purified on neutral Al_2O_3 using dichloromethane as eluent. The desired fractions were collected and evaporated under reduced pressure to yield the desired product as an orange powder (520 mg, 230 μmol, 85% yield). The solid is soluble in all common laboratory solvents except for water.

$[Ru(bpy)_3](NO_3)_2$. $[Ru(bpy)_3](Cl)_2.6H_2O$ (200 mg, 267 mmol, 1.0 eq.) was dissolved in Milli-Q water (20 mL). A solution of silver nitrate ($AgNO_3$, 109 mg, 641 μmol. 2.4 eq.) in milliQ water (5 mL) was added, and the solution was stirred for 10 minutes. The solution is filtered on celite to eliminate colloidal particles of silver chloride. The filtrate was then evaporated under reduced pressure to yield the desired product as an orange powder (170 mg, 245 μmol, 92% yield).

$[Ru(bpy)_3](OTf)_2$. $[Ru(bpy)_3](Cl)_2.6H_2O$ (200 mg, 267 μmol, 1.0 eq.) was dissolved in Milli-Q water (20 mL). A solution of silver trifluoromethanesulfonate (AgOTf, 164 mg, 640 mmol, 2.4 eq.) in milliQ water (5 mL) was added, and the solution was stirred for 10 minutes. The solution is filtered on celite to eliminate the colloidal particles of silver chloride. The filtrate was then evaporated under reduced pressure to yield the desired product as an orange powder in quantitative yield.

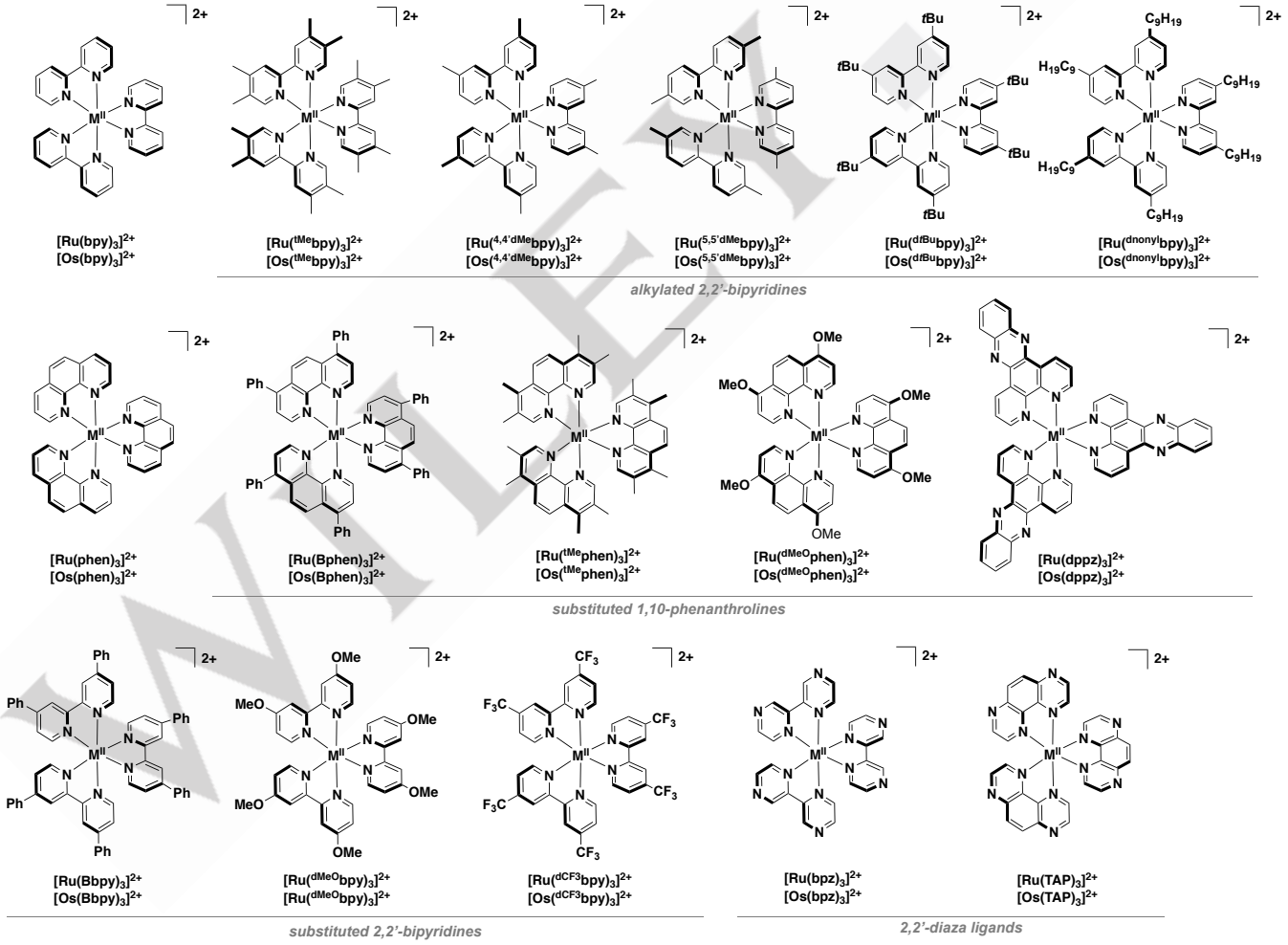

Figure 2. Structures of the Ru(II) and Os(II) photosensitizers investigated in this study.

Results and Discussion

Synthesis

The synthesis of the Ru(II) and Os(II) photosensitizers involved the use of a metal precursor that was either ruthenium trichloride ($RuCl_3.3H_2O$) or ammonium hexachloroosmate ($[OsCl_6](NH_4)_2$), and the latter was itself synthesized from osmium tetroxide and iron(II) chloride in the presence of hydrochloric acid (details described in the experimental procedures). One equivalent of the metal precursor was mixed with 3.5 equivalents of the ligand of interest. In this study the ligands investigated were 2,2'-bipyridine (bpy), 1,10-phenanthroline (phen), 4,7-diphenyl-1,10-phenanthroline (bathophenanthroline, Bphen), 2,2'-bipyrazine (bpz), 1,4,5,8-tetraazaphenanthrene (TAP), 4,4'-di-*tert*-butyl-2,2'-bipyridine (^{dtBu}bpy), 4,4',5,5'-tetramethyl-2,2'-bipyridine (^{tMe}bpy), 4,4'-dimethyl-2,2'-bipyridine ($^{4,4'dMe}$bpy), 5,5'-dimethyl-2,2'-bipyridine ($^{5,5'dMe}$bpy), 4,4'-dinonyl-2,2'-bipyridine (^{dnonyl}bpy), 4,4'-dimethoxy-2,2'-bipyridine (^{dMeO}bpy), 4,4'-bistrifluoromethyl-2,2'-bipyridine (^{dCF3}bpy), 4,7-dimethoxy-1,10-phenanthroline (^{dMeO}phen), 3,4,7,8-tetramethyl-1,10-phenanthroline (^{tMe}phen), 4,4'-diphenyl-2,2'-bipyridine (Bbpy) and dipyrido[3,2-a:2',3'-c]phenazine (dppz). Most of these reactions are described on the gram scale but the reaction can be easily adapted to smaller scales without significant differences in yields. The reaction was carried out in argon-purged ethylene glycol, typically heated at 180 °C for 16 hours for the Ru(II) photosensitizers and at 230 °C for 48 hours for the Os(II) photosensitizers. After the reaction, ion metathesis with excess ammonium hexafluorophosphate yielded the desired photosensitizers. Except for the 2,2'-bipyrazine, dipyrido[3,2-a:2',3'-c]phenazine and the 1,4,5,8-tetraazaphenanthrene ligands, the reaction proceeded smoothly and yielded the desired photosensitizers in moderate to high yields. The photosensitizers could often be purified by simple precipitation in diethyl ether from acetonitrile solutions or by column chromatography when thin-layer chromatography or ^{1}H-NMR measurements indicated the presence of impurities. The synthesis was especially efficient with alkylated 2,2'-bipyridine ligands or electron-withdrawing trifluoromethyl groups. At the same time, the general procedure was not amenable to ligands that were functionalized with groups capable of undergoing (trans)esterification or decarboxylation, such as carboxylic acids, esters, and 4,4'-cyano-2,2'-bipyridine. The synthesis of methoxy-substituted derivatives, i.e., $[Ru(^{dMeO}bpy)_3]^{2+}$, $[Os(^{dMeO}bpy)_3]^{2+}$, $[Ru(^{dMeO}phen)_3]^{2+}$ and $[Os(^{dMeO}phen)_3]^{2+}$ did not proceed well in ethylene glycol and led to a mixture of products that were challenging to separate. Better results were achieved with a solvent mixture of DMF/water/methanol (1:1:1) and a lowered temperature of 140 °C for 60 hours.[73] $[Ru(^{dnonyl}bpy)_3]^{2+}$ and $[Os(^{dnonyl}bpy)_3]^{2+}$ were soluble in diethyl ether and therefore they were purified by column chromatography. Whereas the general procedure worked well for $[Os(phen)_3]^{2+}$ in small scale, the purification was more complicated to perform on a larger scale. Hence, the photosensitizer was isolated as a chloride salt, purified by column chromatography on alumina and then isolated as hexafluorophosphate salt by ion metathesis. The most challenging syntheses were for $[Os(TAP)_3]^{2+}$ and $[Os(bpz)_3]^{2+}$. Whereas the synthesis proceeded efficiently and without issue for the Ru(II) analogues, with Os(II) the synthesis resulted in the formation of various undesired side products and additionally, the desired product proved complicated to isolate. Attempts to decrease the temperature and the concentration or change the osmium source to $OsCl_3$ led to small improvements in the yields. In addition, it was concluded that ion metathesis with ammonium hexafluorophosphate was not optimal for these two complexes, as some of the photosensitizer remained in aqueous solution. Thereby, the isolation and purification processes were optimized. After the reaction, the Os(II) photosensitizer was diluted with water and loaded on an anion exchange chromatography column (Sephadex C-25). The column was first eluted with water to remove neutral impurities and ethylene glycol. The photosensitizer was then purified by eluting it with an aqueous sodium chloride solution of increased concentration. The desired fractions were then collected and evaporated. After anion exchange chromatography, the complex was isolated in methanol, and the desired product was isolated after salt metathesis. We also attempted to obtain $[Os(TAP)_3]^{2+}$ using isolated bis-chelated $[Os(TAP)_2(Cl)_2]$.[81,82] This led to almost identical yields (21% over two steps) but greatly simplified the purification procedure as the product could be readily purified by Sephadex LH20 size exclusion chromatography using methanol as eluent.

The modulation of the ligand scaffold for transition metal complexes offers many opportunities to tune the excited-state properties. Still, the counterion of the charged complex can also influence the chemical properties, i.e., the solubility of the photosensitizer[83] or its photophysical properties.[84,85] Consequently, it is, in some cases, valuable and desirable to exchange the counterion of the respective photosensitizer. Generally, a change of the counterion is performed by solubilizing the complex in a suitable solvent that provides poor solubility after salt metathesis and allows selective precipitation of the product. For instance, during the synthesis, the complexes in the crude reaction mixture are present as chloride salts and then precipitated from aqueous solutions by adding potassium or ammonium hexafluorophosphate. Starting with $[Ru(bpy)_3](Cl)_2$ in aqueous solution, a similar exchange of the counterion is possible to perchlorate (ClO_4^-) by the addition of aqueous perchloric acid (see experimental precautions), to tetrafluoroborate (BF_4^-) by the addition of sodium tetrafluoroborate, to tetrakis[3,5-bis(trifluoromethyl)phenyl]borate (BAr^{F-}) by the addition of sodium tetrakis[3,5-bis(trifluoromethyl)phenyl]borate, to nitrate (NO_3^-) by the addition of silver nitrate or to triflate (OTf^-) by the addition of silver trifluoromethansulfonate. The product is sometimes further purified by additional filtration steps to remove other insoluble salts. The exchange proceeded with yields greater than 80% in all cases. An ion exchange from PF_6^- to chloride is possible by dissolving the photosensitizer in acetone and performing ion metathesis using tetra-*n*-butylammonium chloride (TBACl) in quantitative yields. This procedure for counter-ion exchange, or slight modifications thereof (see SI), was also successfully performed on $[Ru(^{dCF3}bpy)_3]^{2+}$, $[Ru(^{4,4'dMe}bpy)_3]^{2+}$, $[Os(bpy)_3]^{2+}$, $[Os(^{4,4'dMe}bpy)_3]^{2+}$ and $[Os(^{dCF3}bpy)_3]^{2+}$ with good to moderate yields (Table S1). Even if we did not encounter any issue with that series of photosensitizers, it should be noted that silver can also act as an oxidant and as such other cations with low solubility once associated with chloride should be used. Additionally, given the unique solubility of the photosensitizers bearing the 4,4'-dinonyl-2,2'-bipyridine, for example, we believe that such counter-ion exchange could require further optimization for some of the photosensitizers presented in this study.

Photophysical Characterization

Before delving into the photophysical properties of these photosensitizers, it is worth reemphasizing that most of these photosensitizers were already reported in the literature and that the yields reported here for Ru(II) photosensitizers are in line with reported values, but that those for Os(II) are usually greater than values found in the literature. In addition, some photophysical characterizations have also been reported in the past decades and are tabulated in the supporting information (Table S3). Numerous spectroscopic values have been reported in different studies and several are also missing from the literature. As such, the determination of ground and excited-state properties under rigorously identical conditions is of great importance for future development in the field.

All photosensitizers' ground-state UV-visible absorption spectra were recorded in acetonitrile (**Figure 3** and **Figure 4**). The photosensitizers exhibited absorption features that are typical for these photosensitizers, namely absorption bands in the UV region attributed to ligand-centered (LC) transitions and broad absorption bands in the visible part of the spectrum attributed to metal-to-ligand charge transfer (MLCT) transitions.[86] The Ru(II) photosensitizers absorbed light intensely in the 400-480 nm range, with molar absorption coefficients going from 12,000 to 30,000 M^{-1} cm^{-1} (**Table 1**). Whereas most Ru(II) photosensitizers exhibited similar molar absorption coefficients, it should be noted that $[Ru(Bphen)_3]^{2+}$ and $[Ru(Bbpy)_3]^{2+}$ exhibited a molar absorption coefficient in the visible range that was almost twice as large. This is in line with the extended aromatic system afforded by the additional phenyl rings.[87] Additional ligand-centered transitions with molar absorption coefficients greater than 50,000 M^{-1} cm^{-1} were observed at wavelengths more energetic than 300 nm due to π-π* transitions within the ligands (see SI). The Os(II) photosensitizers also absorbed light intensely in the visible range with molar absorption coefficients between 9,000 and 27,000 M^{-1} cm^{-1} and maxima from 400 to 520 nm. These transitions correspond to ^{1}MLCT transitions, whereas transitions assigned to the direct excitation of the broad ^{3}MLCT band occur at wavelengths between 450 and 750 nm.[88] These transitions are observable for Os(II) photosensitizers but not for the Ru(II) analogs due to the increased spin-orbit coupling afforded by the Os(II) metal center.[89] $[Os(Bphen)_3]^{2+}$ and $[Os(Bbpy)_3]^{2+}$ also exhibited a molar absorption coefficient in the visible range that was almost twice as large as the other photosensitizers. Additionally, it was noted that $[Os(bpz)_3]^{2+}$ presented a molar absorption coefficient in the visible range that was smaller than for the other Os(II) photosensitizers, in line with the reported values.[73] Additional ligand-centered transitions with molar absorption coefficients from 40,000 to 125,000 M^{-1} cm^{-1} were also observed for the Os(II) photosensitizers at wavelengths more energetic than 300 nm (see SI).

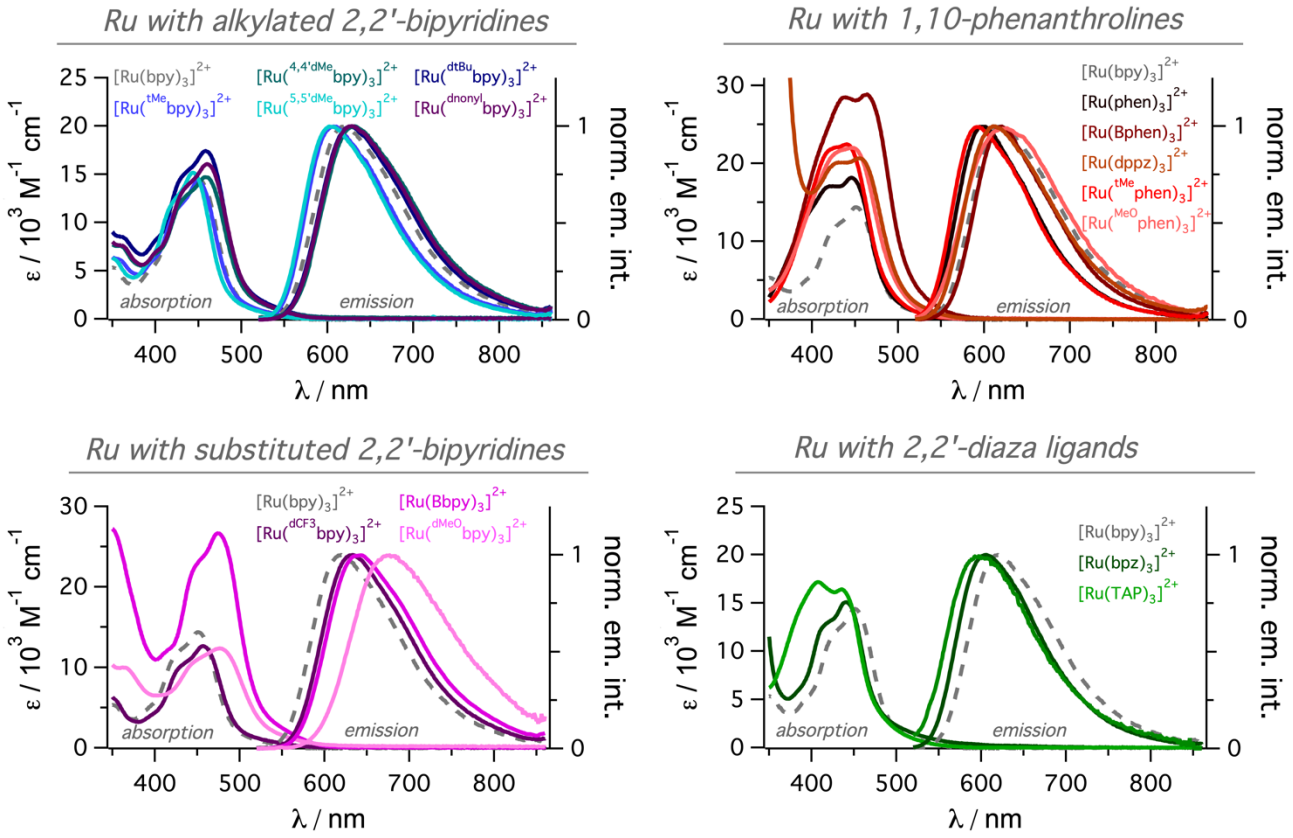

Figure 3. UV-visible absorption (labeled as absorption) and photoluminescence (labeled as emission) spectra for the series of Ru(II) photosensitizers. The complexes are grouped according to structural analogies and $[Ru(bpy)_3]^{2+}$ is shown as reference as dashed traces. The molar absorption coefficients represent an average between 3 to 5 independent measurements. Spectra were recorded at 20 °C in argon-purged acetonitrile. A detailed list of measured values for the individual complexes is also provided in Table 1.

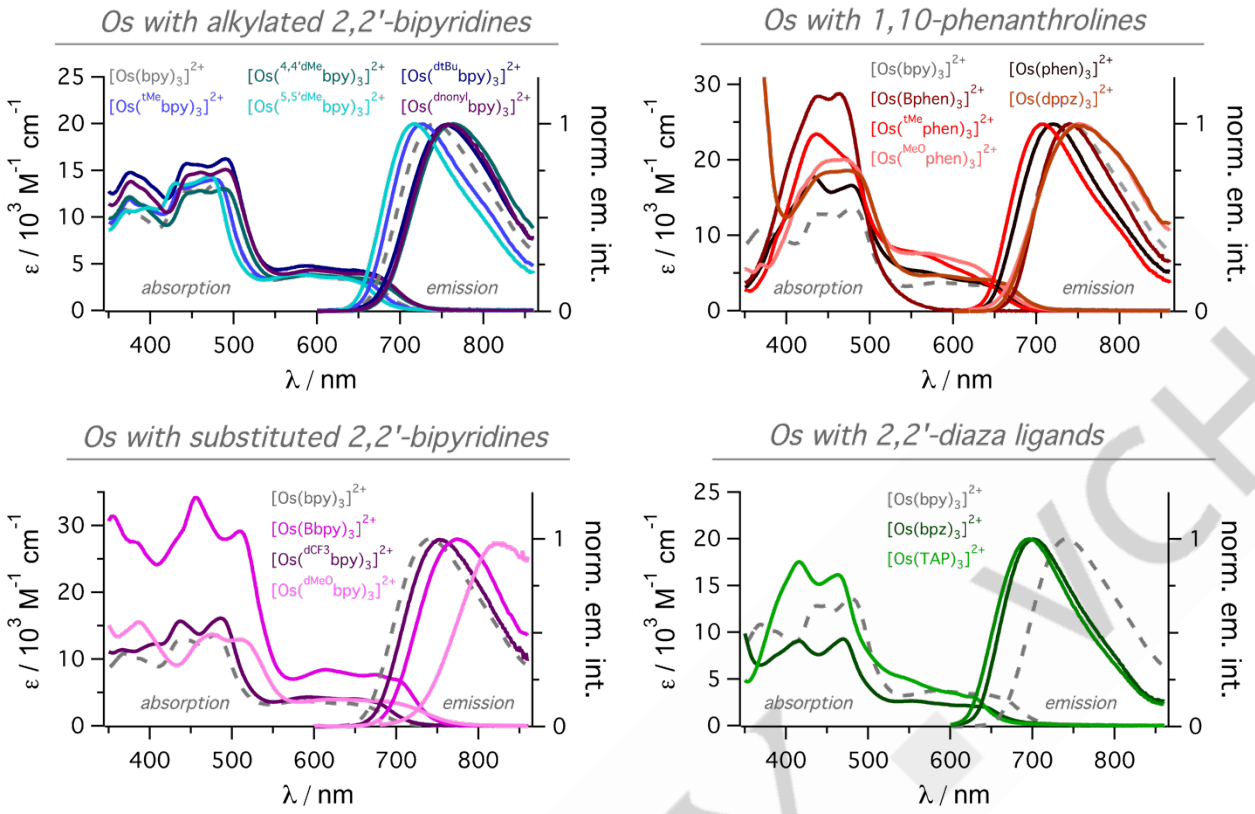

Figure 4. UV-visible absorption (labeled as absorption) and photoluminescence (labeled as emission) spectra for the series of Os(II) photosensitizers. The complexes are grouped according to structural analogies and $[Os(bpy)_3]^{2+}$ is shown as reference as dashed traces. The molar absorption coefficients represent an average between 3 to 5 independent measurements. Spectra were recorded at 20 °C in argon-purged acetonitrile. Detailed list of measured values for the individual complexes are also provided in **Table 1**.

Table 1. Molar absorption coefficients and emission maxima for the Ru(II) and Os(II) photosensitizers. All values were determined in acetonitrile at 20 °C.

	Ruthenium		Osmium	
Photosensitizer	λ (ε) / nm (10^3 M^{-1} cm^{-1})	λ_{em} / nm	λ (ε) / nm (10^3 M^{-1} cm^{-1})	λ_{em} / nm
$[M(bpy)_3]^{2+}$	288 (81.2), 451 (14.4)	620	291 (93.2), 438 (12.8), 481 (13.5), 588 (3.71)	742
$[M(^{tMe}bpy)_3]^{2+}$	292 (84.4), 426 (11.5), 450 (14.2)	608	295 (97.72), 375 (11.9), 438 (13.1), 479 (14.0), 581 (3.91)	727
$[M(^{4,4'dMe}bpy)_3]^{2+}$	287 (89.7), 432 (12.4), 459 (14.7)	632	291 (86.5), 375 (12.1), 460 (12.8), 487 (13.0), 594 (3.84)	764
$[M(^{5,5'dMe}bpy)_3]^{2+}$	294 (95.5), 418 (11.8), 445 (15.2)	605	296 (104), 431 (13.6), 472 (14.3), 581 (3.85)	718
$[M(^{dtBu}bpy)_3]^{2+}$	289 (93.4), 430 (14.7), 459 (17.4)	638	292 (94.4), 376 (13.8), 462 (14.8), 490 (15.1), 599 (4.32)	759
$[M(^{dnonyl}bpy)_3]^{2+}$	289 (88.2), 433 (13.4), 460 (16.1)	628	292 (97.9), 377 (14.8), 446 (15.7), 489 (16.2), 581 (4.77)	727
$[M(phen)_3]^{2+}$	264 (118.6), 448 (18.0)	595	265 (118.7), 432 (17.8), 478 (16.6), 600 (4.21)	721
$[M(Bphen)_3]^{2+}$	278 (148.3), 441 (28.5), 464 (28.9)	620	280 (122.1), 430 (30.3), 500 (26.4), 600 (8.39)	739
$[M(^{tMe}phen)_3]^{2+}$	269 (126), 418 (21.5), 440 (22.7)	594	271 (120.0), 436 (23.1), 563 (7.6)	708
$[M(^{dMeO}phen)_3]^{2+}$	257 (147), 282 (18.0), 445 (22.0)	627	257 (122.0), 308 (22.8), 456 (20.0), 581 (7.30)	752
$[M(dppz)_3]^{2+}$	280 (158), 359 (40.8), 455 (20.7)	610	281 (137.90), 360 (35.95), 470 (18.45), 577 (4.49)	748
$[M(Bbpy)_3]^{2+}$	259 (83.6), 308 (84.8), 475 (26.7)	634	259 (116.8), 457 (34.26), 509 (29.18), 614 (8.43), 675 (7.69)	765
$[M(^{dCF3}bpy)_3]^{2+}$	295 (67.5), 433 (10.3), 456 (12.6)	633	298 (98.3), 437 (15.7), 487 (16.1), 601 (4.29)	752
$[M(^{dMeO}bpy)_3]^{2+}$	276 (57.0), 450 (10.8), 476 (12.2)	675	288 (64.7), 388 (15.6), 477 (13.7), 512 (12.9), 626 (3.97)	823
$[M(bpz)_3]^{2+}$	293 (59.9), 416 (12.7), 440 (15.1)	606	296 (40.3), 416 (9.08), 469 (9.28), 554 (2.64)	703
$[M(TAP)_3]^{2+}$	277 (64.2), 408 (17.2), 436 (16.4)	597	282 (60.2), 416 (17.5), 463 (16.2), 600 (3.54)	699

Visible light excitation of these Ru(II) and Os(II) photosensitizers led to appreciable photoluminescence with maxima centered between 594 and 675 nm for the Ru(II) photosensitizers that were further red-shifted to values between 699 and 823 nm for the Os(II) photosensitizers (**Table 1)**. This is in line with the smaller HOMO-LUMO gap in Os(II) photosensitizers compared to Ru(II) photosensitizers (*vide infra*).

The photoluminescence decay was well described using a first-order kinetic model from which the excited-state lifetime was determined (**Table 2**). Whereas the photoluminescence maxima (**Table 1**) were invariant to whether they were measured under air or argon, the excited-state lifetimes were, in some cases, drastically influenced by oxygen. This is unsurprising as most of these photosensitizers can transfer energy to ground-state triplet oxygen and exhibit excited-state lifetime greater than 50 ns.[90] For Ru(II) photosensitizers, the excited-state lifetime recorded under air varied over one order of magnitude from 51 ns for $[Ru(TAP)_3]^{2+}$ to 580 ns for $[Ru(^{dCF3}bpy)_3]^{2+}$. Under argon, the excited-state lifetime of $Ru(TAP)_3]^{2+}$ remained essentially unchanged, but the one of $[Ru(^{dCF3}bpy)_3]^{2+}$ was extended to 1510 ns. These changes

in lifetime are in agreement with different bimolecular quenching rate constants with dissolved oxygen in acetonitrile with a limited concentration of 1.9 mM under ambient air.[11] These rate constants range from $2x10^8$ to $9.3x10^9$ $M^{-1}s^{-1}$ for all investigated complexes (Table S2). The most drastic influence of dissolved oxygen was observed for $[Ru(Bphen)_3]^{2+}$ that evolved from 165 ns under air to 5140 ns and argon. This is in agreement with a more highly delocalized excited state due to the phenyl rings of bathophenanthroline,[91] thus extending the excited-state lifetime and providing a longer time to react with dissolved oxygen.[92–94] Hence, this photosensitizer would be highly suitable for applications working *via* $^1O_2$ formation. The excited-state lifetimes of the Os(II) photosensitizers were much shorter, and were as such less dependent on the presence of dissolved oxygen (**Table 2**). Similar to the Ru(II) photosensitizers, the shortest lifetimes (e.g. $[Os(^{dMeO}bpy)_3]^{2+}$) were hardly affected by the presence of oxygen, while for $[Os(phen)_3]^{2+}$ about 70% of the excited-state lifetime was quenched by oxygen. The differences between osmium and ruthenium complexes is once again in line with the energy gap law (*vide infra*) and with the fact that osmium photosensitizers, unlike certain Ru(II) analogues, do not cross to the metal-centered (^{3}MC) state, which is often considered too high in energy to be reached at room temperature (*vide infra*).[79,95]

The radiative (k_r) and non-radiative (k_{nr}) rate constants were calculated based on the experimentally determined values using equations 1 and 2.[86]

$$k_r = \frac{\Phi}{\tau_0} \quad \text{Eq. 1}$$

$$k_{nr} = \frac{1}{\tau_0} - k_r \quad \text{Eq. 2}$$

The values are tabulated in **Table 2**. Under aerated conditions, k_{nr} was always at least one order of magnitude larger than k_r. Under deaerated conditions, significant changes were found between the individual photosensitizers (**Table 2** and **Figure 5**).

Table 2. Excited-state lifetimes (τ_0), photoluminescence quantum yields (Φ) as well as the radiative (k_r) and non-radiative (k_{nr}) rate constants for the Ru(II) and Os(II) photosensitizers in air and under argon. All values were determined in acetonitrile at 20 °C.

Photosensitizer	$\tau_{0,air}$ / ns	Φ_{air} / %	$k_{r,air}$ / 10^5 s^{-1}	$k_{nr,air}$ / 10^6 s^{-1}	$\tau_{0,Ar}$ / ns	Φ_{Ar} / %	$k_{r,Ar}$ / 10^5 s^{-1}	$k_{nr,Ar}$ / 10^6 s^{-1}
Ruthenium								
$[Ru(bpy)_3]^{2+}$	160	1.80 [96,a]	1.12	6.13	950	9.37 (±0.14)	0.99	0.96
$[Ru(^{tMe}bpy)_3]^{2+}$	55	0.74 (±0.01)	1.34	17.9	330	4.65 (±0.13)	1.40	2.16
$[Ru(^{4,4'dMe}bpy)_3]^{2+}$	105	1.41(±0.05)	1.36	9.52	780	9.52 (±0.11)	1.22	1.16
$[Ru(^{5,5'dMe}bpy)_3]^{2+}$	90	0.80 (±0.03)	0.90	11.2	445	3.80 (±0.06)	0.85	2.16
$[Ru(^{dtBu}bpy)_3]^{2+}$	105	1.39 (±0.01)	1.34	9.50	870	12.6 (±0.6)	1.45	1.01
$[Ru(^{dnonyl}bpy)_3]^{2+}$	100	1.47 (±0.03)	1.49	9.96	755	9.55 (±0.27)	1.27	1.20
$[Ru(phen)_3]^{2+}$	100	0.70 (±0.01)	0.72	10.2	375	2.87 (±0.19)	0.77	2.60
$[Ru(Bphen)_3]^{2+}$	165	1.37 (±0.01)	0.84	5.98	5140	51.3 (±0.7)[b]	1.00	0.09
$[Ru(^{tMe}phen)_3]^{2+}$	50	0.32 (±0.01)	0.62	19.2	685	4.08 (±0.09)	0.59	1.40
$[Ru(^{dMeO}phen)_3]^{2+}$	25	0.16 (±0.01)	0.59	37.0	40	0.37 (±0.01)	0.88	23.7
$[Ru(dppz)_3]^{2+}$	215	0.87 (±0.03)	0.41	46.1	840	3.63 (±0.06)	0.43	1.15
$[Ru(Bbpy)_3]^{2+}$	190	3.43 (±0.07)	1.78	5.00	1590	29.3 (±0.5)[b]	1.85	0.45
$[Ru(^{dMeO}bpy)_3]^{2+}$	65	0.69 (±0.02)	1.06	15.3	220	2.26 (±0.11)	1.03	4.46
$[Ru(^{dCF3}bpy)_3]^{2+}$	580	6.50 (±0.06)	1.13	1.62	1510	15.7 (±0.3)	1.04	0.56
$[Ru(bpz)_3]^{2+}$	540	3.53 (±0.10)	0.66	1.79	775	4.90 (±0.16)	0.63	1.23
$[Ru(TAP)_3]^{2+}$	50	0.46 (±0.01)	0.90	19.6	50	0.58 (±0.03)	1.11	19.1
Osmium								
$[Os(bpy)_3]^{2+}$	39	0.33 (±0.01)	0.84	25.4	55	0.50 [96,c]	0.92	18.3
$[Os(^{tMe}bpy)_3]^{2+}$	37	0.44 (±0.02)	1.17	26.5	110	1.37 (±0.04)	1.25	8.99
$[Os(^{4,4'dMe}bpy)_3]^{2+}$	24	0.19 (±0.01)	0.78	40.9	33	0.26 (±0.01)	0.80	30.6
$[Os(^{5,5'dMe}bpy)_3]^{2+}$	47	0.56 (±0.01)	1.18	21.0	145	1.86 (±0.04)	1.29	6.80
$[Os(^{dtBu}bpy)_3]^{2+}$	31	0.28 (±0.01)	0.88	31.3	51	0.48 (±0.02)	0.94	19.5
$[Os(^{dnonyl}bpy)_3]^{2+}$	33	0.25 (±0.01)	0.76	30.2	39	0.35 (±0.01)	0.91	25.9
$[Os(phen)_3]^{2+}$	61	0.60 (±0.01)	0.98	16.2	210	2.10 (±0.02)	1.02	4.75
$[Os(Bphen)_3]^{2+}$	78	1.14 (±0.04)	1.45	12.5	230	3.54 (±0.05)	1.52	4.14
$[Os(^{tMe}phen)_3]^{2+}$	41	0.56 (±0.01)	1.35	23.9	390	5.41 (±0.05)	1.38	2.42
$[Os(^{dMeO}phen)_3]^{2+}$	27	0.17 (±0.01)	0.62	36.2	53	0.36 (±0.01)	0.68	18.8
$[Os(dppz)_3]^{2+}$	11	0.12 (±0.01)	1.06	88.4	12	0.15 (±0.01)	1.27	84.6
$[Os(Bbpy)_3]^{2+}$	43	0.74 (±0.02)	1.69	22.7	60	1.04 (±0.03)	1.74	16.6
$[Os(^{dMeO}bpy)_3]^{2+}$	5	0.016 (±0.001)	0.34	213	5	0.017 (±0.001)	0.34	200
$[Os(^{dCF3}bpy)_3]^{2+}$	57	0.51 (±0.01)	0.90	17.6	63	0.58 (±0.02)	0.92	15.8
$[Os(bpz)_3]^{2+}$	180	1.77 (±0.03)	0.98	5.42	230	2.27 (±0.02)	1.00	4.31
$[Os(TAP)_3]^{2+}$	310	3.35 (±0.03)	1.09	3.16	470	5.11 (±0.06)	1.09	2.03

All measurements were performed in acetonitrile at room temperature with hexafluorophosphate as counterion. a) Aerated $[Ru(bpy)_3](PF_6)_2$ serves as a reference for the determination of all other aerated (Φ_{air}) and deaerated quantum yields (Φ_{Ar}) with ruthenium complexes.[96,97] b) Deaerated $[Ru(bpy)_3](PF_6)_2$ serves as a reference. c) Deaerated $[Os(bpy)_3](PF_6)_2$ serves as a reference for the determination of all other aerated (Φ_{air}) and deaerated quantum yields (Φ_{Ar}) with osmium complexes.[96,98]

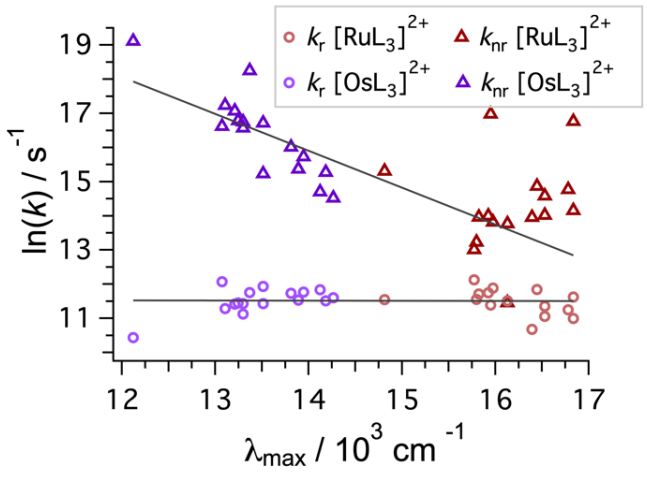

Figure 5. Plot of the natural logarithm of the radiative (k_r,cicles) and non-radiative (k_{nr}, triangles) rate constants for all Ru(II) and Os(II) photosensitizers in purple and red respectively as a function of the steady-state photoluminescence maxima λ_{max}. Values were determined in argon-purged acetonitrile at 20 °C. Fitting line for non-radiative rate constants include all complexes with emission maxima below 16,500 cm^{-1}. A detailed list of measured values for the individual complexes is also provided in **Table 2**.

Plotting the non-radiative rate constant against the emission maxima of the photosensitizers, a trend to higher non-radiative rate constants with lower triplet energies of the excited state (= higher maximum of emission energy in wavenumbers in **Figure 5**) is found. Hence, the linear relationship indicated that the non-radiative rate constant followed Jortner's energy gap law[99] (Figure 5). The linear correlation for the Os(II) and Ru(II) photosensitizers remains until 16,500 cm^{-1}, where deviations start to appear (red data points in **Figure 5**). The most prominent deviation is for [Ru(TAP)$_3$]$^{2+}$. The non-radiative rate constant is often used to describe all the processes that participate in the non-radiative deactivation of the excited state.[6,49,100] In the specific case of [Ru(TAP)$_3$]$^{2+}$, the use of three 1,4,5,8-tetraazaphenanthrene ligands decreases the gap between the ^{3}MLCT excited state and the ^{3}MC state, such that crossing towards this ^{3}MC state becomes statistically more probable. This excited state is often associated with ligand-loss chemistry, which occurs via a non-radiative process. As such, it is therefore not surprising to see that photosensitizer fall outside of the linear correlation. Although photostability measurements were not performed, the lack of correlation for photosensitizers at wavenumber greater than 16,500 cm^{-1} could also originate from changes in the ^{3}MLCT-^{3}MC crossing.

The steady-state photoluminescence was also recorded at 77 K in butyronitrile glasses and resulted in a hypsochromic shift of the photoluminescence spectra and the observation of well-resolved vibronic structures. A double-mode Franck-Condon (FC) lineshape analysis was used to fit the photoluminescence spectra that were used to obtain the energy of the transition between the lowest vibrational levels of the ground and excited states (E_{00}), the energy of the weighted-average, ground-state, acceptor vibrational mode in cm^{-1} ($\hbar\omega_M$), the Huang Rhys factor (S_M) which is a measure of the geometric distortion between the ground and excited states, and the spectral full-width at half-maximum ($\Delta\nu_{1/2}$). These results are tabulated in **Table 3**. Overall, the average acceptor vibrational mode was around 1300-1400 cm^{-1} and around 400-500 cm^{-1}, which are in line with an average acceptor vibrational mode related to several C–C and C–N stretching modes of the ligand. The Huang-Rhys factor was always larger for Ru(II) photosensitizers than for their Os(II) analogs, thus implying that the excited state of Os(II) photosensitizers is less distorted from their ground state compared to the Ru(II) analogs. However, this observation was not unexpected as it had already been shown that the Huang-Rhys factor varies linearly with E_{00} for photosensitizers that share similar excited-state characters. Indeed, the ground and excited-state mixing should be more efficient as E_{00} decreases, and thus, the amount of charge transferred to the π* orbitals of the ligand should decrease alongside the distortion, leading to smaller values of S_M.[101–104]

Table 3. Emission spectral fitting parameters and Huang-Rhys parameters.[a]

	Ruthenium						Osmium					
Photosensitizer	E_{00} / cm^{-1}	$\hbar\omega_1$ / cm^{-1}	S_1	$\hbar\omega_1$ / cm^{-1}	S_2	$\nu_{1/2}$ / cm^{-1}	E_{00} / cm^{-1}	$\hbar\omega_1$ / cm^{-1}	S_1	$\hbar\omega_1$ / cm^{-1}	S_2	$\nu_{1/2}$ / cm^{-1}
[M(bpy)$_3$]$^{2+}$	17400	1390	0.98	440	1.08	605	14220	1330	0.51	380	0.71	670
[M(^{tMe}bpy)$_3$]$^{2+}$	17580	1380	0.95	440	0.76	655	14230	1360	0.48	450	0.47	695
[M($^{4,4'dMe}$bpy)$_3$]$^{2+}$	16940	1380	1.08	470	0.81	790	14340	1370	0.38	590	0.30	700
[M($^{5,5'dMe}$bpy)$_3$]$^{2+}$	17540	1430	0.87	680	0.54	750	13900	1400	0.59	570	0.60	670
[M(^{dtBu}bpy)$_3$]$^{2+}$	17580	1390	0.93	470	0.93	655	14400	1380	0.45	500	0.48	720
[M(^{dnonyl}bpy)$_3$]$^{2+}$	17300	1410	0.93	460	0.83	645	14010	1330	0.48	380	0.54	730
[M(phen)$_3$]$^{2+}$	17660	1410	0.74	480	0.65	720	14510	1410	0.46	390	0.66	800
[M(Bphen)$_3$]$^{2+}$	16960	1440	0.69	530	0.62	690	14000	1320	0.43	410	0.55	580
[M(^{tMe}phen)$_3$]$^{2+}$	17880	1380	0.88	450	0.95	615	14780	1380	0.46	500	0.47	680
[M(^{dMeO}phen)$_3$]$^{2+}$	17680	1410	1.14	590	0.50	815	14340	1380	0.63	270	0.60	870
[M(dppz)$_3$]$^{2+}$	17380	1390	0.87	570	0.51	910	14250	1390	0.52	310	0.63	860
[M(Bbpy)$_3$]$^{2+}$	16710	1410	0.76	440	0.60	650	13600	1180	0.39	370	0.50	610
[M(^{dMeO}bpy)$_3$]$^{2+}$	16470	1390	1.05	470	0.80	850	12740	1540	0.58	540	0.28	945
[M(^{dCF3}bpy)$_3$]$^{2+}$	16830	1420	0.84	480	0.87	620	16830	1420	0.84	480	0.87	620
[M(bpz)$_3$]$^{2+}$	17580	1370	1.03	500	0.74	710	14670	1290	0.55	530	0.40	775
[M(TAP)$_3$]$^{2+}$	18000	1370	0.90	440	1.01	615	14980	1390	0.43	400	0.67	755

[a] E_{00}: Energy of the transition between the lowest vibrational levels of the ground and excited state. $\hbar\omega$: Energy of the weighted-average acceptor vibrational mode 1 ($\hbar\omega_1$) and 2 ($\hbar\omega_2$). S: The Huang-Rhys factor, associated with the reorganization energy and frequency of the quantum mode 1 (S_1) and 2 (S_2). $\nu_{1/2}$: The full-width at half-max of the transitions. [b] $E_{0,0}$ in eV is provided in **Table 2**.

Electrochemical Characterization

The ground state redox properties of the Ru(II) and Os(II) photosensitizers were investigated by cyclic voltammetry in acetonitrile (**Table 3**). The metal-centered oxidations occurred at potentials that were centered between 0.92 V and >2.1 V *vs* SCE with the Ru(II) photosensitizers. These potentials were consistently shifted to more negative values by about 500 mV for the Os(II) photosensitizers (blue data points in Figure 6), i.e., with values that ranged from 0.39 V to 1.54 V *vs* SCE. Electron-donating substituents, like in the case of $[Ru(^{dMeO}bpy)_3]^{2+}$ and $[Os(^{dMeO}bpy)_3]^{2+}$ led to photosensitizers that were easily oxidized ($E_{1/2}(M^{III/II})$ = 0.92 V and 0.39 V *vs* SCE). Similarly, the introduction of electron-withdrawing groups, like $[Ru(^{dCF3}bpy)_3]^{2+}$ and $[Os(^{dCF3}bpy)_3]^{2+}$, shifted the oxidation potential to more positive values ($E_{1/2}(M^{III/I})$ = 1.70 V and 1.29 V *vs* SCE). Modification of the ligand backbone to reach more π-accepting ligands, such as 2,2'-bipyrazine or 1,4,5,8-tetraazaphenanthrene led to the most positively-shifted oxidation potentials for $[Os(bpz)_3]^{2+}$ (1.54 V *vs* SCE) and $[Os(TAP)_3]^{2+}$ (1.53 V *vs* SCE) respectively, and values of 1.97 V and >2.1 V vs SCE for the Ru(II) analogs. In line with a mainly ligand-centered reduction, these potentials were similar for the ground state complexes, whether coordinated to the Ru(II) or Os(II) center (orange data points in **Figure 6**).

The excited-state redox potentials (**Table 4**) were calculated using equations 3 and 4 where $E_{1/2}(*PS^{3+/2+})$ is the excited-state oxidation potential, $E_{1/2}(*PS^{2+/+})$ is the excited-state reduction potential, and E_{00} is the energy of the transition between the lowest vibrational levels of the ground and excited states, determined from steady-state photoluminescence at 77K.

$$E_{1/2}(*PS^{3+/2+}) = E_{1/2}(PS^{3+/2+}) - E_{00} \quad \text{Eq. 3}$$

$$E_{1/2}(*PS^{2+/+}) = E_{1/2}(PS^{2+/+}) + E_{00} \quad \text{Eq. 4}$$

Ligands bearing electron-donating groups typically displayed $E_{1/2}(*PS^{3+/2+})$ that were more negative, with the most reducing photosensitizers for oxidative electron transfer being $[Os(^{dMeO}phen)_3]^{2+}$ with $E_{1/2}(*Os^{3+/2+})$ = –1.35 V *vs* SCE and $[Ru(^{dMeO}phen)_3]^{2+}$ with $E_{1/2}(*Ru^{3+/2+})$ of –1.24 V *vs* SCE. It is worth mentioning that the Os(II) photosensitizers provide the possibility of being excited with less energetic wavelengths as they absorb throughout the visible range.[34,39,73]

Table 4. Ground and excited-state redox potentials of the indicated Ru(II) and Os(II) photosensitizers.[a]

Photosensitizer	$E_{1/2}(PS^{3+/2+})$ / V *vs* SCE	$E_{1/2}(PS^{2+/+})$ / V *vs* SCE	E_{00} / eV	$E_{1/2}(*PS^{3+/2+})$ / V *vs* SCE	$E_{1/2}(*PS^{2+/+})$ / V *vs* SCE	$E_{1/2}(PS^{3+/2+})$ V *vs* SCE	$E_{1/2}(PS^{2+/+})$ / V *vs* SCE	E_{00} / eV	$E_{1/2}(*PS^{3+/2+})$ / V *vs* SCE	$E_{1/2}(*PS^{2+/+})$ / V *vs* SCE
	Ruthenium					Osmium				
$[M(bpy)_3]^{2+}$	+1.27	–1.34	2.16	–0.88	+0.82	+0.84	–1.28	1.76	–0.92	+0.48
$[M(^{tMe}bpy)_3]^{2+}$	+1.01	–1.63	2.18	–1.17	+0.55	+0.57	–1.56	1.78	–1.21	+0.22
$[M(^{4,4'dMe}bpy)_3]^{2+}$	+1.11	–1.46	2.10	–0.99	+0.64	+0.67	–1.39	1.72	–1.05	+0.33
$[M(^{5,5'dMe}bpy)_3]^{2+}$	+1.17	–1.52	2.17	–1.00	+0.66	+0.73	–1.43	1.79	–1.06	+0.36
$[M(^{dtBu}bpy)_3]^{2+}$	+1.12	–1.45	2.18	–1.06	+0.73	+0.69	–1.37	1.76	–1.07	+0.39
$[M(^{dnonyl}bpy)_3]^{2+}$	+1.13	–1.44	2.14	–1.01	+0.71	+0.68	–1.37	1.79	–1.06	+0.37
$[M(phen)_3]^{2+}$	+1.28	–1.37	2.19	–0.91	+0.82	+0.84	–1.28	1.80	–0.96	+0.52
$[M(Bphen)_3]^{2+}$	+1.23	–1.31	2.10	–0.87	+0.80	+0.80	–1.23	1.74	–0.94	+0.51
$[M(^{tMe}phen)_3]^{2+}$	+1.07	–1.60	2.22	–1.15	+0.62	+0.61	–1.67	1.83	–1.23	+0.16
$[M(^{dMeO}phen)_3]^{2+}$	+0.95	–1.63	2.19	–1.24	+0.57	+0.43	–1.61	1.78	–1.35	+0.17
$[M(dppz)_3]^{2+}$	+1.41	–0.91	2.15	–0.75.	+1.25	+0.97	–0.91	1.77	–0.80	+0.85
$[M(Bbpy)_3]^{2+}$	+1.21	–1.25	2.07	–0.86	+0.83	+0.81	–1.18	1.69	–0.89	+0.51
$[M(^{dMeO}bpy)_3]^{2+}$	+0.92	–1.50	2.04	–1.12	+0.56	+0.39	–1.44	1.58	–1.19	+0.14
$[M(^{dCF3}bpy)_3]^{2+}$	+1.70	–0.86	2.09	–0.38	+1.23	+1.29	–0.74	1.70	–0.41	+0.96
$[M(bpz)_3]^{2+}$	+1,97	–0.74	2.18	–0.21	+1.44	+1.54	–0.81	1.82	–0.28	+1.01
$[M(TAP)_3]^{2+}$	> +2.1	–0.76	2.23	>–0.1	+1.48	+1.53	–0.67	1.86	–0.33	+1.18

[a] Electrochemical data (in V *vs* SCE) of the indicated Ru(II) and Os(II) photosensitizers (2 mM) recorded in argon-purged acetonitrile with tetrabutylammonium hexafluorophosphate (0.1 M) as supporting electrolyte with a scan rate of 0.1 V s^{-1} to 0.3 V s^{-1} depending on the complex. The E_{00} values were determined from steady-state photoluminescence recorded at 77K.[105] Ground- and excited-state redox potential can be estimated *vs* NHE by adding +0.247 V or *vs* Ag/AgCl (saturated KCl) by adding +0.044V.

Unsurprisingly, ligands bearing electron-accepting groups or with increased π-accepting character resulted in photosensitizers with the most positive $E_{1/2}(*PS^{2+/+})$. In combination with their relatively long excited-state lifetime, $*[Ru(bpz)_3]^{2+}$ (1.44 V *vs* SCE) and to a lesser extent $*[Ru(TAP)_3]^{2+}$ (1.48 V *vs* SCE) represented the most promising photosensitizers for reductive excited-state electron transfer. Similar $E_{1/2}(*PS^{2+/+})$ could not be obtained using Os(II) photosensitizers, where the most positive potential was determined at 1.18 V *vs* SCE for $[Os(TAP)_3]^{2+}$. Thus, whereas similar excited-state oxidation potentials can be obtained for Os(II) and Ru(II) photosensitizer, the Ru(II) photosensitizers can reach excited-state reduction potentials that are on average 440 mV more positive than the Os(II) analogues. This is further visualized in **Figure 6**. Note however that an excited-state reduction potential of 1.18 V *vs* SCE for $[Os(TAP)_3]^{2+}$ is still sufficient to activate biomolecules or iodide, amongst others, and could thus be used to perform interesting photoredox transformations using red light irradiation.[38,73,106,107]

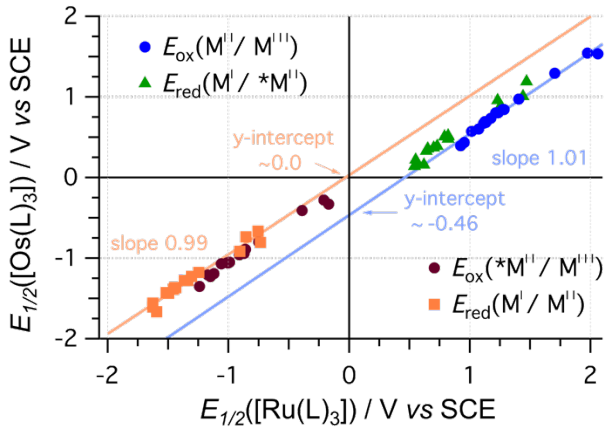

Figure 6. Electrochemical correlation between the Ru(II) and Os(II) photosensitizers in the ground and excited states.

Variable Temperature Measurements

Finally, time-resolved photoluminescence at different temperatures were performed on the prototypical $[Ru(bpy)_3]^{2+}$ and $[Os(bpy)_3]^{2+}$ photosensitizers as well as with $Ru(bpz)_3]^{2+}$, $[Os(bpz)_3]^{2+}$, $Ru(TAP)_3]^{2+}$ and $[Os(TAP)_3]^{2+}$. The experiments were carried out in argon purged butyronitrile with a temperature range from 173 K to 373 K (**Figure 7**).

The photophysical scheme of $[Ru(bpy)_3]^{2+}$ is well established with a thermally equilibrated excited state that, in fact, corresponds to three closely lying triplet metal-to-ligand charge transfer (^{3}MLCT) excited states.[108] In addition to direct radiative and non-radiative decay to the ground state, these ^{3}MLCT excited states can deactivate *via* thermally activated processes, *i.e.* through population of an upper-lying metal-centered state (^{3}MC) or population of a fourth ^{3}MLCT.[109–112] The excited-state lifetime was the longest at 173 K and gradually decreased as the temperature increased. The excited-state lifetime was well described using single-exponential decays throughout the investigated temperature range. The changes in excited-state lifetimes with temperature (**Figure 7**) were well modeled using equation 5, where k_{dr} and k_{dnr} are the activationless direct radiative and non-radiative decay rate constants of the three closely spaced thermally equilibrated ^{3}MLCT states back to the ground state.[49,112,113]

$$\frac{1}{\tau} = k_{dr} + k_{dnr} + k_{3_{MC}} + k_{3_{MLCT}} = k_{dr} + k_{dnr} + A_{3_{MC}} e^{\left(\frac{-E_{3_{MC}}}{RT}\right)} + A_{3_{MLCT}} e^{\left(\frac{-E_{3_{MLCT}}}{RT}\right)} \quad \text{Eq. 5}$$

Altogether, the results presented herein allow us to generate what is considered a "classical" Latimer diagram for the ground and excited-state potentials of all investigated complexes, similar to $[Os(bpy)_3]^{2+}$ and $[Ru(bpy)_3]^{2+}$ in **Figure 8**. The Latimer diagram was created using values gathered in **Table 4**. Together with the variable temperature measurements, the typical photophysical scheme for the Ru(II) and Os(II) photosensitizers can be developed (**Figure 8**).[109,111,112] Regarding the photophysical scheme, light excitation leads to the formation of a ^{1}MLCT excited state that undergoes intersystem crossing to the ^{3}MLCT manifold.[114] In the case of Os(II) photosensitizers, the increased spin-orbit coupling allows direct excitation of the ground state into the ^{3}MLCT manifold using red light irradiation. The ^{3}MLCT manifold then deactivates following multiple radiative and non-radiative pathways. Non-radiative decay rate constants have been shown to decrease linearly as the photoluminescence maxima shifted to a more energetic wavelength. The radiative decay rate constant remained only slightly affected by the chemical modifications introduced in the ligand scaffold.

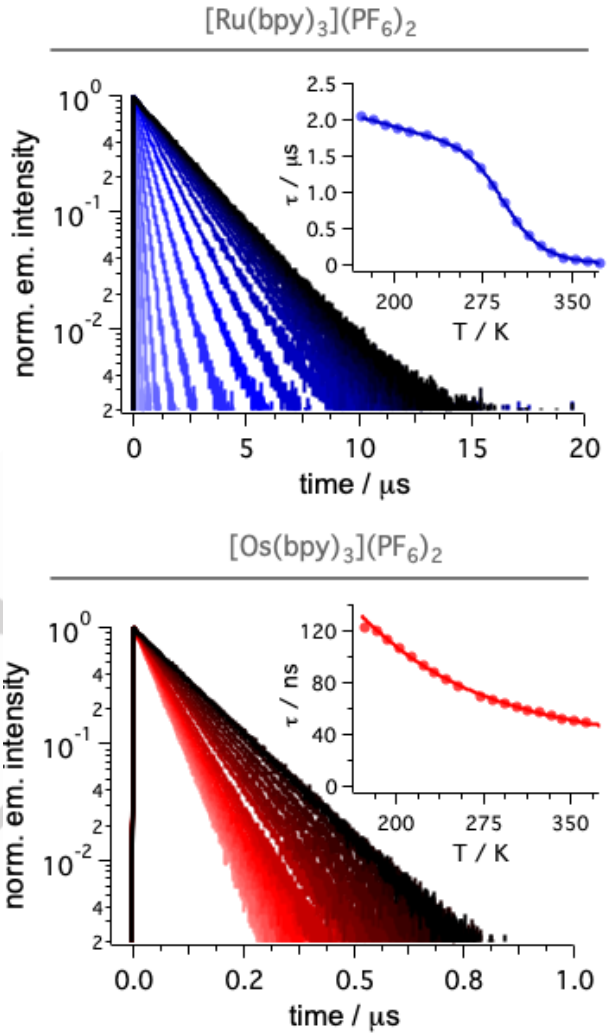

Figure 7. Time-resolved photoluminescence spectra recorded at 620 nm ($[Ru(bpy)_3]^{2+}$, top) and at 740 nm ($[Os(bpy)_3]^{2+}$, bottom) recorded in argon-purged butyronitrile at temperatures ranging from 173 K to 373 K. The relative energy between the excited states remains constant within the range of temperatures studied. The other parameters, i.e. k_{3MC} and k_{3MLCT} are the temperature dependent deactivation rate constants associated with the thermal population of the ^{3}MC state (k_{3MC}) or 4th ^{3}MLCT (k_{3MLCT}), respectively. These deactivation pathways were characterized by the pre-exponential factors A_{3MC} and A_{3MLCT}, as well as the corresponding activation energies, E_{3MC} and E_{3MLCT}.

In both $[Os(bpy)_3]^{2+}$ and $[Ru(bpy)_3]^{2+}$, variable temperature measurements indicated that the ^{3}MLCT manifold also deactivated *via* crossing to a 4th ^{3}MLCT, with activation energies of 370 cm^{-1} and 405 cm^{-1} and preexponential factors of 7.63 x10^7 s^{-1} and 1.33 x10^6 s^{-1} for $[Os(bpy)_3]^{2+}$ and $[Ru(bpy)_3]^{2+}$, respectively. Both the magnitude of the activation energy and the preexponential factor are in line with typical values for crossing towards the 4th ^{3}MLCT.[49,111,112,115] For $[Ru(bpy)_3]^{2+}$, the variable temperature measurements also indicated that deactivation *via*

crossing to the metal-centered state (MC),[108,116] often called a ligand-field state, also occurred efficiently, with an activation energy of 3870 cm^{-1}. It should be emphasized that this value corresponds to the activation energy to cross to that ^{3}MC state but does not provide the actual energy/position of the ^{3}MC level. Crossing to that state was also characterized by the sizeable preexponential factor of 9.49 $x10^{13}$ s^{-1}. Interestingly, for $[Os(bpy)_3]^{2+}$, crossing to the ^{3}MC state was not observed through these variable temperature measurements.[79,117]

For $Ru(bpz)_3]^{2+}$, the activation energy to cross to the ^{3}MC state increased to 4510 cm^{-1} with a large pre-exponential factor of 4.27 $x10^{15}$ s^{-1}, indicating the probable lack of photostability. Rigidification of the structure using $Ru(TAP)_3]^{2+}$ led to a decrease in the activation energy to cross to the ^{3}MC state to 3550 cm^{-1} with a pre-exponential factor of 1.15 $x10^{15}$ s^{-1}. For both complexes, crossing to the 4th MLCT also occurred with activation energies of 320 cm^{-1} and 390 cm^{-1} and preexponential factors of 1.92 $x10^6$ s^{-1} and 1.01 $x10^6$ s^{-1} for $[Ru(bpz)_3]^{2+}$ and $Ru(TAP)_3]^{2+}$, respectively. Crossing to the ^{3}MC state was not observed for $[Os(TAP)_3]^{2+}$ and $[Os(bpz)_3]^{2+}$ that only deactivated via crossing to the 4th MLCT. This occurred with activation energies of 440 cm^{-1} and 380 cm^{-1} and preexponential factors of 2.45 $x10^7$ s^{-1} and 8.68 $x10^6$ s^{-1} for $[Os(bpz)_3]^{2+}$ and $Os(TAP)_3]^{2+}$, respectively . These results likely accounts for the overall greater photostability of Os(II) photosensitizers compared to Ru(II) photosensitizers.[39,118]

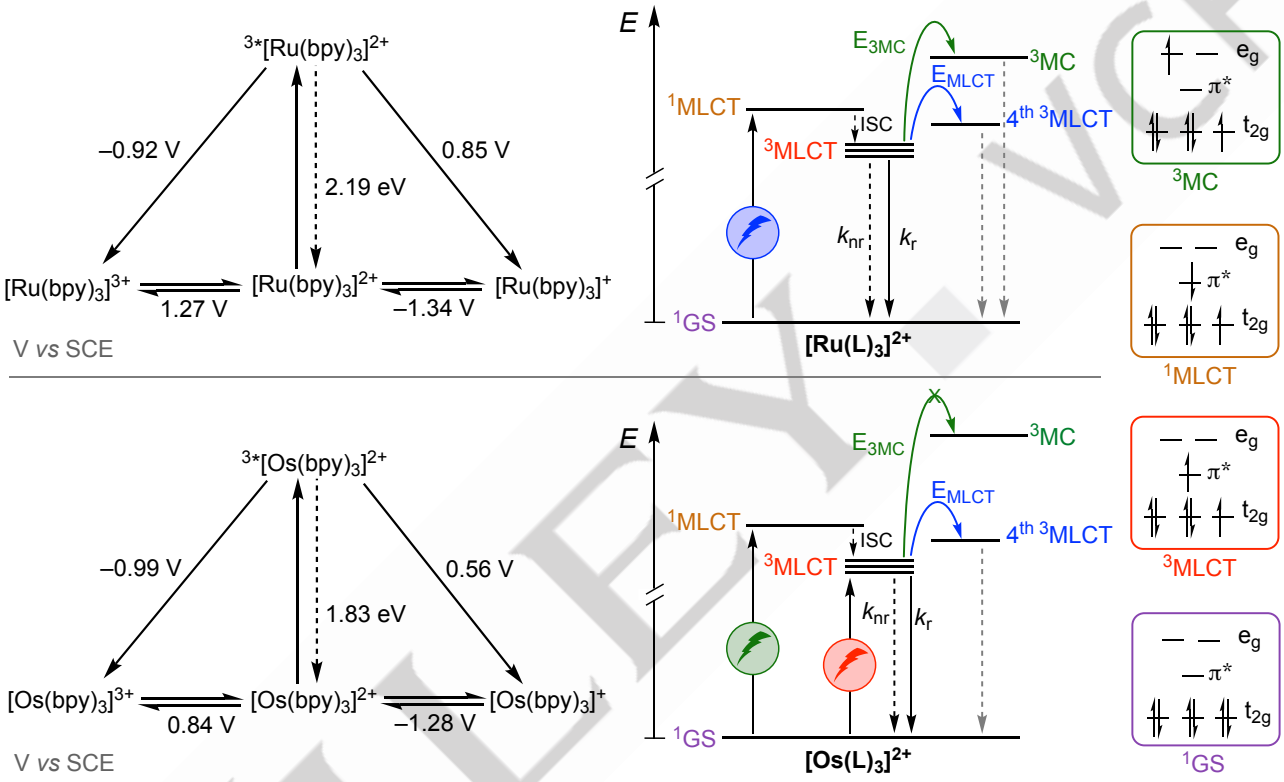

Figure 8. Classical Latimer diagram for $[Os(bpy)_3]^{2+}$ and $[Ru(bpy)_3]^{2+}$ (left) as well as a proposed photophysical scheme and electronic configuration of the different energy states for the Ru(II) and Os(II) photosensitizers (right).

Conclusion

Here, we propose a systematic study focusing on the synthesis and photophysical investigation of 32 photosensitizers based on Ru(II) or Os(II) metal centers. The study was centered around the synthesis of homoleptic photosensitizers using ligands that are either commercially available or obtainable in large scale using between one (4,4'-bistrifluoromethyl-2,2'-bipyridine, 2,2'-bipyrazine and 4,4'-diphenyl-2,2'-bipyridine) and four (1,4,5,8-tetraazaphenanthrene) synthetic steps.[119] Most of the photosensitizers were obtained in high yields, with minimal need for lengthy purification processes, which contributes to their use for photoredox transformations. The ground and excited-state properties of all photosensitizers were characterized in the present study and compared with the literature (see SI). The Ru(II) photosensitizers exhibited intense absorption in the blue spectral range whereas the Os(II) counterparts absorbed intensely as well in that part of the spectrum, but their absorption additionally further extended towards the red. Most of the time, the excited-state lifetimes of the Ru(II) photosensitizers were longer than the Os(II) analogs. An exception is $[Os(TAP)_3]^{2+}$, which exhibited a longer excited-state lifetime than $[Ru(TAP)_3]^{2+}$. This was due to the inability of $[Os(TAP)_3]^{2+}$ to cross to the ^{3}MC state,[79] thereby suppressing one of the excited-state non-radiative decay processes. This allows us to foresee interesting avenues for $[Os(TAP)_3]^{2+}$ for photoredox catalysis as $[Ru(TAP)_3]^{2+}$ tends to be less photostable.[68,120,121] In addition, the excited-state redox potentials were determined for all the photosensitizers and were shown to span a wide range. In line with literature reports,[6,109] variable temperature measurements show much more significant changes in excited-state lifetimes for Ru(II)-based photosensitizers compared to the Os(II) analog due to the

additional deactivation via the non-radiative ^{3}MC state. This implies a more negligible temperature dependence of the Os(II) photosensitizers and could potentially be relevant to understand different reactivities or stabilities in light-driven applications. Determining pertinent properties in one study allows us to directly compare the investigated photosensitizers in a systematic fashion. The complete characterization of Os(II), as well as Ru(II) photosensitizers presented herein, can provide guidance to selecting proper candidates for envisioned applications.
Furthermore, with the growing interest in machine learning and artificial intelligence, using datasets determined under identical conditions is highly desirable and sought after.[122] While the present study only focused on homoleptic photosensitizers, the results offer clear boundaries within which the properties can be fine-tuned through the development of heteroleptic photosensitizers.[73,123–127]

Supporting Information

Additional characterization, photophysical characterization, molar absorption coefficient, variable temperature measurements, quenching with oxygen, ^{1}H NMR spectra, and comparison with literature. The authors have cited additional references within the Supporting Information.[11,39,75,78,79,86,91,96,97,123,128,129,65,130–139,66,140–147,67–70,72,73]

Acknowledgments

This work was supported by the Fonds de la Recherche Scientifique (F.R.S.-FNRS) under CDR grant no. 40020332 (L.T.-G.). L.T.-G. is a Chercheur Qualifié of the Fonds de la Recherche Scientifique – FNRS. F. G. is a Chargé de Recherches of the Fonds de la Recherche Scientifique (FNRS). A.R., N.C., M.D. and M.V.W.-L. thank the Belgian National Funds for Scientific Research (F.R.S.-FNRS) for their Fund for Research Training in Industry and Agriculture (FRIA) PhD grant. All the authors gratefully acknowledge the UCLouvain for financial support. This publication benefited from the support of the Walloon Region as part of the financing of the FRFS-WEL-T strategic axis.

Keywords: Photochemistry • Photophysics • Osmium • Ruthenium • Franck-Condon

References

1 N. A. Romero and D. A. Nicewicz, *Chem. Rev.*, 2016, **116**, 10075–10166.
2 E. Speckmeier, T. G. Fischer and K. Zeitler, *J. Am. Chem. Soc.*, 2018, **140**, 15353–15365.
3 C. Fischer, C. Kerzig, B. Zilate, O. S. Wenger and C. Sparr, *ACS Catal.*, 2020, **10**, 210–215.
4 T. Bortolato, S. Cuadros, G. Simionato and L. Dell'Amico, *Chem. Commun.*, 2022, **58**, 1263–1283.
5 Y. Wu, D. Kim and T. S. Teets, *Synlett*, 2022, **33**, 1154–1179.
6 A. Juris, V. Balzani, F. Barigelletti, S. Campagna, P. Belser and A. von Zelewsky, *Coord. Chem. Rev.*, 1988, **84**, 85–277.
7 J. Beaudelot, S. Oger, S. Peruško, T.-A. Phan, T. Teunens, C. Moucheron and G. Evano, *Chem. Rev.*, 2022, **122**, 16365–16609.
8 W. R. Kitzmann and K. Heinze, *Angew. Chem. Int. Ed.*, 2023, **62**, e202213207.
9 C. Cavedon, S. Gisbertz, S. Reischauer, S. Vogl, E. Sperlich, J. H. Burke, R. F. Wallick, S. Schrottke, W. H. Hsu, L. Anghileri, Y. Pfeifer, N. Richter, C. Teutloff, H. Müller-Werkmeister, D. Cambié, P. H. Seeberger, J. Vura-Weis, R. M. van der Veen, A. Thomas and B. Pieber, *Angew. Chem. Int. Ed.*, 2022, **61**, e202211433.
10 C. S. Day, Á. Rentería-Gómez, S. J. Ton, A. R. Gogoi, O. Gutierrez and R. Martin, *Nat. Catal.*, 2023, **6**, 244–253.
11 M. Montalti, A. Credi, L. Prodi and M. T. Gandolfi, *Handbook of Photochemistry*, CRC Press: Taylor & Francis Group, Boca Raton, FL, USA, 3rd edn., 2006.
12 C. Förster and K. Heinze, *Chem. Soc. Rev.*, 2020, **49**, 1057–1070.
13 M. W. Mara, K. A. Fransted and L. X. Chen, *Coord. Chem. Rev.*, 2015, **282**–**283**, 2–18.
14 M. S. Lazorski and F. N. Castellano, *Polyhedron*, 2014, **82**, 57–70.
15 M. D. Woodhouse and J. K. McCusker, *J. Am. Chem. Soc.*, 2020, **142**, 16229–16233.
16 A. Y. Chan, A. Ghosh, J. T. Yarranton, J. Twilton, J. Jin, D. M. Arias-Rotondo, H. A. Sakai, J. K. McCusker and D. W. C. MacMillan, *Science*, 2023, **382**, 191–197.
17 K. Teegardin, J. I. Day, J. Chan and J. Weaver, *Org. Process Res. Dev.*, 2016, **20**, 1156–1163.
18 N. Tomar, A. Agrawal, V. S. Dhaka and P. K. Surolia, *Sol. Energy*, 2020, **207**, 59–76.
19 M. M. Alowakennu, A. Ghosh and J. K. McCusker, *J. Am. Chem. Soc.*, 2023, **145**, 20786–20791.
20 T. H. Bürgin, F. Glaser and O. S. Wenger, *J. Am. Chem. Soc.*, 2022, **144**, 14181–14194.
21 F. P. Dwyer and E. C. Gyarfas, *Nature*, 1950, 166, 481.
22 F. H. Burstall, F. P. Dwyer and E. C. Gyarfas, *J. Chem. Soc.*, 1950, 953.
23 W. W. Brandt, F. P. Dwyer and E. C. Gyarfas, *Chem. Rev.*, 1954, **54**, 959–1017.
24 F. E. Lytle and D. M. Hercules, *J. Am. Chem. Soc.*, 1969, **91**, 253–257.
25 F. H. Burstall, *J. Chem. Soc.*, 1936, 173.
26 C. Pandya and A. Sivaramakrishna, *Coord. Chem. Rev.*, 2024, **504**, 215655.
27 P. T. Cesana, B. X. Li, S. G. Shepard, S. I. Ting, S. M. Hart, C. M. Olson, J. I. Martinez Alvarado, M. Son, T. J. Steiman, F. N. Castellano, A. G. Doyle, D. W. C. MacMillan and G. S. Schlau-Cohen, *Chem*, 2022, **8**, 174–185.
28 C. Kerzig and O. S. Wenger, *Chem. Sci.*, 2018, **9**, 6670–6678.
29 M. S. Coles, G. Quach, J. E. Beves and E. G. Moore, *Angew. Chem. Int. Ed.*, 2020, **59**, 9522–9526.
30 A. Rilak Simović, R. Masnikosa, I. Bratsos and E. Alessio, *Coord. Chem. Rev.*, 2019, **398**, 113011.
31 N. Toupin, M. K. Herroon, R. P. Thummel, C. Turro, I. Podgorski, H. Gibson and J. J. Kodanko, *Chem. Eur. J.*, 2022, **28**, e202104430.
32 N. Y. Puttaswamy, P. Mahanta, P. Sarma, C. Medhi, S. M. A. Kaid, B. Kullaiah, D. Basumatary and B. A. Manjasetty, *Chem. Biol. Drug Des.*, 2023, **102**, 1506–1520.
33 A. Gandioso, K. Purkait and G. Gasser, *Chimia*, 2021, **75**, 845–855.
34 Y. Wei, Y. Li, M. Zheng, X. Zhou, Y. Zou and C. Yang, *Adv. Opt.*

Mater., 2020, **8**, 1902157.

35 R. Haruki, Y. Sasaki, K. Masutani, N. Yanai and N. Kimizuka, *Chem. Commun.*, 2020, **56**, 7017–7020.

36 D. Liu, Y. Zhao, Z. Wang, K. Xu and J. Zhao, *Dalton Trans.*, 2018, **47**, 8619–8628.

37 B. D. Ravetz, N. E. S. Tay, C. L. Joe, M. Sezen-Edmonds, M. A. Schmidt, Y. Tan, J. M. Janey, M. D. Eastgate and T. Rovis, *ACS Cent. Sci.*, 2020, **6**, 2053–2059.

38 S. L. Goldschmid, N. E. Soon Tay, C. L. Joe, B. C. Lainhart, T. C. Sherwood, E. M. Simmons, M. Sezen-Edmonds and T. Rovis, *J. Am. Chem. Soc.*, 2022, **144**, 22409–22415.

39 F. Glaser and O. S. Wenger, *Chem. Sci.*, 2023, **14**, 149–161.

40 G. Han, G. Li, J. Huang, C. Han, C. Turro and Y. Sun, *Nat. Commun.*, 2022, **13**, 2288.

41 T. Swetha, K. R. Reddy and S. P. Singh, *Chem. Rec.*, 2015, **15**, 457–474.

42 T. Kinoshita, J. I. Fujisawa, J. Nakazaki, S. Uchida, T. Kubo and H. Segawa, *J. Phys. Chem. Lett.*, 2012, **3**, 394–398.

43 S. A. M. Wehlin, L. Troian-Gautier, A. B. Maurer, M. K. Brennaman and G. J. Meyer, *J. Chem. Phys.*, 2020, **153**, 054307.

44 S. Lazic, P. Kaspler, G. Shi, S. Monro, T. Sainuddin, S. Forward, K. Kasimova, R. Hennigar, A. Mandel, S. McFarland and L. Lilge, *Photochem. Photobiol.*, 2017, **93**, 1248–1258.

45 J. A. Roque, P. C. Barrett, H. D. Cole, L. M. Lifshits, G. Shi, S. Monro, D. Von Dohlen, S. Kim, N. Russo, G. Deep, C. G. Cameron, M. E. Alberto and S. A. McFarland, *Chem. Sci.*, 2020, **11**, 9784–9806.

46 A. Mani, T. Feng, A. Gandioso, R. Vinck, A. Notaro, L. Gourdon, P. Burckel, B. Saubaméa, O. Blacque, K. Cariou, J. Belgaied, H. Chao and G. Gasser, *Angew. Chem. Int. Ed.*, 2023, **62**, e202218347.

47 H. Madec, F. Figueiredo, K. Cariou, S. Roland, M. Sollogoub and G. Gasser, *Chem. Sci.*, 2022, **14**, 409–442.

48 M. D. Pozza, P. Mesdom, A. Abdullrahman, T. D. Prieto Otoya, P. Arnoux, C. Frochot, G. Niogret, B. Saubaméa, P. Burckel, J. P. Hall, M. Hollenstein, C. J. Cardin and G. Gasser, *Inorg. Chem.*, 2023, **62**, 18510–18523.

49 S. Cerfontaine, S. A. M. Wehlin, B. Elias and L. Troian-Gautier, *J. Am. Chem. Soc.*, 2020, **142**, 5549–5555.

50 L. Schmid, C. Kerzig, A. Prescimone and O. S. Wenger, *JACS Au*, 2021, jacsau.1c00137.

51 K. Eastham, P. A. Scattergood, D. Chu, R. Z. Boota, A. Soupart, F. Alary, I. M. Dixon, C. R. Rice, S. J. O. Hardman and P. I. P. Elliott, *Inorg. Chem.*, 2022, **61**, 19907–19924.

52 H. Song, A. Amati, A. Pannwitz, S. Bonnet and L. Hammarström, *J. Am. Chem. Soc.*, 2022, **144**, 19353–19364.

53 L. Candish, K. D. Collins, G. C. Cook, J. J. Douglas, A. Gómez-Suárez, A. Jolit and S. Keess, *Chem. Rev.*, 2022, **122**, 2907–2980.

54 P. Li, J. A. Terrett and J. R. Zbieg, *ACS Med. Chem. Lett.*, 2020, **11**, 2120–2130.

55 L. Flamigni, A. Barbieri, C. Sabatini, B. Ventura and F. Barigelletti, in *Photochemistry and Photophysics of Coordination Compounds II. Topics in Current Chemistry*, eds. V. Balzani and S. Campagna, Springer, Berlin, Heidelberg, 2007, vol. 281, pp. 143–203.

56 J. L. Kahl, K. Hanck and K. DeArmond, *J. Inorg. Nucl. Chem.*, 1979, **41**, 495–502.

57 L. Wang, P. Cui, B. Liu, S. Kilina and W. Sun, *Dalton Trans.*, 2018, **47**, 13776–13780.

58 S. D. Lies, S. Lin and T. P. Yoon*, in *Organic Syntheses*, 2017, pp. 178–199.

59 R. M. O'Donnell, R. N. Sampaio, G. Li, P. G. Johansson, C. L. Ward and G. J. Meyer, *J. Am. Chem. Soc.*, 2016, **138**, 3891–3903.

60 B. T. Patterson and F. Richard Keene, *Inorg. Chem.*, 1998, **37**, 645–650.

61 R. Bevernaegie, S. A. M. Wehlin, E. J. Piechota, M. Abraham, C. Philouze, G. J. Meyer, B. Elias and L. Troian-Gautier, *J. Am. Chem. Soc.*, 2020, **142**, 2732–2737.

62 R. Nasielski-Hinkens and M. Benedek-Vamos, *J. Chem. Soc. Perkin Trans. 1*, 1975, 1229.

63 Z. Molphy, A. Prisecaru, C. Slator, N. Barron, M. McCann, J. Colleran, D. Chandran, N. Gathergood and A. Kellett, *Inorg. Chem.*, 2014, **53**, 5392–5404.

64 W. S. Han, J. K. Han, H. Y. Kim, M. J. Choi, Y. S. Kang, C. Pac and S. O. Kang, *Inorg. Chem.*, 2011, **50**, 3271–3280.

65 P. J. Steel, F. Lahousse, D. Lerner and C. Marzin, *Inorg. Chem.*, 1983, **22**, 1488–1493.

66 N. Alatrash, F. H. Issa, N. S. Bawazir, S. J. West, K. E. Van Manen-Brush, C. P. Shelor, A. S. Dayoub, K. A. Myers, C. Janetopoulos, E. A. Lewis and F. M. MacDonnell, *Chem. Sci.*, 2020, **11**, 264–275.

67 D. M. Schultz, J. W. Sawicki and T. P. Yoon, *Beilstein J. Org. Chem.*, 2015, **11**, 61–65.

68 R. Z. Boota, S. J. O. Hardman, G. P. Ashton, C. R. Rice, P. A. Scattergood and P. I. P. Elliott, *Inorg. Chem.*, 2021, **60**, 15768–15781.

69 D. van der Westhuizen, K. G. von Eschwege and J. Conradie, *Electrochim. Acta*, 2019, **320**, 134540.

70 L. Kohler, L. Nease, P. Vo, J. Garofolo, D. K. Heidary, R. P. Thummel and E. C. Glazer, *Inorg. Chem.*, 2017, **56**, 12214–12223.

71 Y. Yamazaki, J. Rohacova, K. Koike and O. Ishitani, *JACS Au*, 2021, **1**, 294–307.

72 S. Bhand, D. N. Lande, E. Pereira, S. P. Gejji, T. Weyhermüller, D. Chakravarty, V. G. Puranik and S. Salunke-Gawali, *Polyhedron*, 2019, **164**, 96–107.

73 S. L. Goldschmid, E. Bednářová, L. R. Beck, K. Xie, N. E. S. Tay, B. D. Ravetz, J. Li, C. L. Joe and T. Rovis, *Synlett*, 2022, **33**, 247–258.

74 S. V. Kumar, S. O. Scottwell, E. Waugh, C. J. McAdam, L. R. Hanton, H. J. L. Brooks and J. D. Crowley, *Inorg. Chem.*, 2016, **55**, 9767–9777.

75 S. Roy, E. Colombo, R. Vinck, C. Mari, R. Rubbiani, M. Patra and G. Gasser, *ChemBioChem*, 2020, **21**, 2966–2973.

76 C. Parella, A. Blanquer, S. Sinha, E. Hümpfner, J. Hernando, E. Mora, X. Fontrodona, Z. Kelemen, C. Nogués, R. Núñez and I. Romero, *Dye. Pigm.*, 2024, , DOI:10.1016/j.dyepig.2024.111985.

77 F. P. J. Dwyer and J. T. Hogarth, *J. Proc. R. Soc. New South Wales*, 1951, **84**, 194–195.

78 Y. Wei, M. Zheng, L. Chen, X. Zhou and S. Liu, *Dalton Trans.*, 2019, **48**, 11763–11771.

79 S. Content and A. K. De Mesmaeker, *J. Chem. Soc. - Faraday Trans.*, 1997, **93**, 1089–1094.

80 S. Jansod, L. Wang, M. Cuartero and E. Bakker, *Chem. Commun.*, 2017, **53**, 10757–10760.

81 F. Dröge, F. F. Noakes, S. A. Archer, S. Sreedharan, A. Raza, C. C. Robertson, S. Macneil, J. W. Haycock, H. Carson, A. J. H. M. Meijer, C. G. W. Smythe, J. Bernardino De La Serna, B. Dietzek-Ivanšić and J. A. Thomas, *J. Am. Chem. Soc.*, 2021, **143**, 20442–

20453.

82 M. Stitch, R. Z. Boota, A. S. Chalkley, T. D. Keene, J. C. Simpson, P. A. Scattergood, P. I. P. Elliott and S. J. Quinn, *Inorg. Chem.*, 2022, **61**, 14947–14961.

83 D. Jespersen, B. Keen, J. I. Day, A. Singh, J. Briles, D. Mullins and J. D. Weaver, *Org. Process Res. Dev.*, 2019, **23**, 1087–1095.

84 J. D. Earley, A. Zieleniewska, H. H. Ripberger, N. Y. Shin, M. S. Lazorski, Z. J. Mast, H. J. Sayre, J. K. McCusker, G. D. Scholes, R. R. Knowles, O. G. Reid and G. Rumbles, *Nat. Chem.*, 2022, **14**, 746–753.

85 E. P. Farney, S. J. Chapman, W. B. Swords, M. D. Torelli, R. J. Hamers and T. P. Yoon, *J. Am. Chem. Soc.*, 2019, **141**, 6385–6391.

86 D. M. Arias-Rotondo and J. K. McCusker, *Chem. Soc. Rev.*, 2016, **45**, 5803–5820.

87 K. Kalyanasundaram, *Coord. Chem. Rev.*, 1982, **46**, 159–244.

88 A. B. Maurer and G. J. Meyer, *J. Am. Chem. Soc.*, 2020, **142**, 6847–6851.

89 D. Kumaresan, K. Shankar, S. Vaidya and R. H. Schmehl, *Top. Curr. Chem.*, 2007, **281**, 101–142.

90 A. A. Abdel-Shafi, D. R. Worrall and A. Y. Ershov, *Dalton Trans.*, 2004, 30.

91 N. H. Damrauer, T. R. Boussie, M. Devenney and J. K. McCusker, *J. Am. Chem. Soc.*, 1997, **119**, 8253–8268.

92 M. C. DeRosa and R. J. Crutchley, *Coord. Chem. Rev.*, 2002, **233–234**, 351–371.

93 A. C. Sell, J. C. Wetzel, M. Schmitz, A. W. Maijenburg, G. Woltersdorf, R. Naumann and C. Kerzig, *Dalton Trans.*, 2022, **51**, 10799–10808.

94 S. Guo, R. Tao and J. Zhao, *RSC Adv.*, 2014, **4**, 36131–36139.

95 J. P. Lecomte, A. Kirsch-De Mesmaeker and G. Orellana, *J. Phys. Chem.*, 1994, **98**, 5382–5388.

96 A. M. Brouwer, *Pure Appl. Chem.*, 2011, **83**, 2213–2228.

97 K. Suzuki, A. Kobayashi, S. Kaneko, K. Takehira, T. Yoshihara, H. Ishida, Y. Shiina, S. Oishi and S. Tobita, *Phys. Chem. Chem. Phys.*, 2009, **11**, 9850–9860.

98 E. M. Kober, J. V. Caspar, R. S. Lumpkin and T. J. Meyer, *J. Phys. Chem.*, 1986, **90**, 3722–3734.

99 A. Nitzan, S. Mukamel and J. Jortner, *J. Chem. Phys.*, 1975, **63**, 200–207.

100 V. Balzani and S. Campagna, *Photochemistry and Photophysics of Coordination Compounds I*, Springer, Berlin, Heidelberg, 2007.

101 J. P. Claude and T. J. Meyer, *J. Phys. Chem.*, 1995, **99**, 51–54.

102 T. A. Heimer, C. A. Bignozzi and G. J. Meyer, *J. Phys. Chem.*, 1993, **97**, 11987–11994.

103 L. A. Worl, R. Duesing, P. Chen, L. Della Ciana and T. J. Meyer, *J. Chem. Soc. Dalt. Trans.*, 1991, 849–858.

104 J. V. Caspar and T. J. Meyer, *J. Am. Chem. Soc.*, 1983, **105**, 5583–5590.

105 J. R. Lakowicz, *Principles of Fluorescence Spectroscopy*, Springer US, Boston, MA, 2006.

106 B. Elias and A. Kirsch-De Mesmaeker, *Coord. Chem. Rev.*, 2006, **250**, 1627–1641.

107 L. Troian-Gautier, M. D. Turlington, S. A. M. Wehlin, A. B. Maurer, M. D. Brady, W. B. Swords and G. J. Meyer, *Chem. Rev.*, 2019, **119**, 4628–4683.

108 D. W. Thompson, A. Ito and T. J. Meyer, *Pure Appl. Chem.*, 2013, **85**, 1257–1305.

109 R. S. Lumpkin, E. M. Kober, L. A. Worl, Z. Murtaza and T. J. Meyer, *J. Phys. Chem.*, 1990, **94**, 239–243.

110 F. Barigelletti, V. Balzani, A. Juris, V. Balzani, P. Belser and A. Von Zelewsky, *J. Phys. Chem.*, 1987, **91**, 1095–1098.

111 T. C. Motley, L. Troian-Gautier, M. K. Brennaman and G. J. Meyer, *Inorg. Chem.*, 2017, **56**, 13579–13592.

112 S. Cerfontaine, L. Troian-Gautier, S. A. M. Wehlin, F. Loiseau, E. Cauët and B. Elias, *Dalton Trans.*, 2020, **49**, 8096–8106.

113 J. Van Houten and R. J. Watts, *J. Am. Chem. Soc.*, 1976, **98**, 4853–4858.

114 N. H. Damrauer, G. Cerullo, A. Yeh, T. R. Boussie, C. V. Shank and J. K. McCusker, *Chemtracts*, 1998, **11**, 621–625.

115 R. M. O'Donnell, P. G. Johansson, M. Abrahamsson and G. J. Meyer, *Inorg. Chem.*, 2013, **52**, 8282–8282.

116 D. Hernández-Castillo, I. Eder and L. González, *Coord. Chem. Rev.*, 2024, **510**, 215819.

117 Y. Sasaki, N. Yanai and N. Kimizuka, *Inorg. Chem.*, 2022, **61**, 5982–5990.

118 Z. J. Fuller, W. D. Bare, K. A. Kneas, W. Y. Xu, J. N. Demas and B. A. DeGraff, *Anal. Chem.*, 2003, **75**, 2670–2677.

119 S. De Kreijger, E. Cauët, B. Elias and L. Troian-Gautier, *Dalton Trans.*, 2024, 10270–10284.

120 F. Alary, M. Boggio-Pasqua, J. L. Heully, C. J. Marsden and P. Vicendo, *Inorg. Chem.*, 2008, **47**, 5259–5266.

121 A. Masschelein, L. Jacquet, A. Kirsch-De Mesmaeker and J. Nasielski, *Inorg. Chem.*, 1990, **29**, 855–860.

122 N. Artrith, K. T. Butler, F. X. Coudert, S. Han, O. Isayev, A. Jain and A. Walsh, *Nat. Chem.*, 2021, **13**, 505–508.

123 Z. Mahmood, J. He, S. Cai, Z. Yuan, H. Liang, Q. Chen, Y. Huo, B. König and S. Ji, *Chem. Eur. J.*, 2023, **29**, e202202677.

124 N. A. Till, L. Tian, Z. Dong, G. D. Scholes and D. W. C. MacMillan, *J. Am. Chem. Soc.*, 2020, **142**, 15830–15841.

125 P. A. Scattergood, A. Sinopoli and P. I. P. Elliott, *Coord. Chem. Rev.*, 2017, **350**, 136–154.

126 R. E. Holmlin, J. A. Yao and J. K. Barton, *Inorg. Chem.*, 1999, **38**, 174–189.

127 S. A. E. Omar, P. A. Scattergood, L. K. McKenzie, C. Jones, N. J. Patmore, A. J. H. M. Meijer, J. A. Weinstein, C. R. Rice, H. E. Bryant and P. I. P. Elliott, *Inorg. Chem.*, 2018, **57**, 13201–13212.

128 W. J. Dressick, J. Cline, J. N. Demas and B. A. DeGraff, *J. Am. Chem. Soc.*, 1986, **108**, 7567–7574.

129 L. F. Cooley, C. E. L. Headford, C. M. Elliott and D. F. Kelley, *J. Am. Chem. Soc.*, 1988, **110**, 6673–6682.

130 A. Ito, N. Kobayashi and Y. Teki, *Inorg. Chem.*, 2017, **56**, 3794–3808.

131 Y. Yamazaki, T. Onoda, J. Ishikawa, S. Furukawa, C. Tanaka, T. Utsugi and T. Tsubomura, *Front. Chem.*, 2019, , DOI:10.3389/fchem.2019.00288.

132 C.-Y. Ding, J.-Y. Shao, Z.-L. Gong, Y.-W. Zhong and J. Yao, *J. Mater. Chem. C*, 2021, **9**, 16485–16494.

133 L. Petermann, R. Staehle, M. Pfeifer, C. Reichardt, D. Sorsche, M. Wächtler, J. Popp, B. Dietzek and S. Rau, *Chem. Eur. J.*, 2016, **22**, 8240–8253.

134 R. Staehle, C. Reichardt, J. Popp, D. Sorsche, L. Petermann, K. Kastner, C. Streb, B. Dietzek and S. Rau, *Eur. J. Inorg. Chem.*, 2015, **2015**, 3932–3939.

135 D. Rota Martir, M. Averardi, D. Escudero, D. Jacquemin and E.

Zysman-Colman, *Dalton Trans.*, 2017, **46**, 2255–2262.

136 E. Rajkumar, P. M. Mareeswaran and S. Rajagopal, *Photochem. Photobiol. Sci.*, 2014, **13**, 1261–1269.

137 L. J. Boudreau, T. L. Clarke, A. H. Murray, K. N. Robertson, T. S. Cameron and M. A. S. Aquino, *Inorg. Chim. Acta*, 2013, **394**, 152–158.

138 M. Mariappan, M. Suenaga, A. Mukhopadhyay, P. Raghavaiah and B. G. Maiya, *Inorg. Chim. Acta*, 2011, **376**, 340–349.

139 S.-F. Wang, X.-P. Cao and Y. Li, *Angew. Chem. Int. Ed.*, 2017, **56**, 13809–13813.

140 M. K. Brennaman, J. H. Alstrum-Acevedo, C. N. Fleming, P. Jang, T. J. Meyer and J. M. Papanikolas, *J. Am. Chem. Soc.*, 2002, **124**, 15094–15098.

141 A. M. Carver and M. J. Knapp, *Polyhedron*, 2008, **27**, 3313–3317.

142 H. B. Ross, M. Boldaji, D. P. Rillerm, C. B. Blanton and R. P. White, *Inorg. Chem.*, 1989, **28**, 1013–1021.

143 S. Kajouj, L. Marcélis, V. Lemaur, D. Beljonne and C. Moucheron, *Dalton Trans.*, 2017, **46**, 6623–6633.

144 B. Maubert, N. D. McClenaghan, M. T. Indelli and S. Campagna, *J. Phys. Chem. A*, 2003, **107**, 447–455.

145 G. F. Strouse, J. R. Schoonover, R. Duesing, S. Boyde, W. E. Jones and T. J. Meyer, *Inorg. Chem.*, 1995, **34**, 473–487.

146 R. D. Schmidt, C. A. Kent, J. J. Concepcion, W. Lin, T. J. Meyer and M. D. E. Forbes, *Dalton Trans.*, 2014, **43**, 17729–17739.

147 S. A. Poteet, M. B. Majewski, Z. S. Breitbach, C. A. Griffith, S. Singh, D. W. Armstrong, M. O. Wolf and F. M. MacDonnell, *J. Am. Chem. Soc.*, 2013, **135**, 2419–2422.

Entry for the Table of Contents

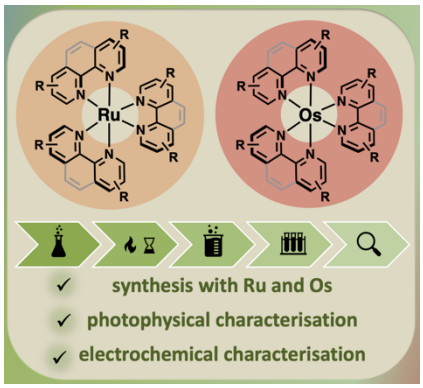

The synthesis of polypyridyl ruthenium- and osmium-based photosensitizers is reported alongside their photophysical and electrochemical characterizations. Both metal centers are compared in detail, and the comparison is discussed.

Institute and/or researcher Twitter usernames: @LudoTroian